Volcanotectonic interactions between inclined sheets, dykes, and faults at the Santorini Volcano, Greece

Kyriaki Drymoni[a*], John Browning[b, c], Agust Gudmundsson[a]

a Department of Earth Sciences, Queen's Building, Royal Holloway University of London Egham, Surrey TW20 0EX, UK

b Department of Mining Engineering and Department of Structural and Geotechnical Engineering, Pontificia Universidad Católica de Chile, Santiago, Chile

c Centro de Excelencia en Geotermia de los Andes (CEGA), Chile

* Corresponding author

E-mail address: Kyriaki.Drymoni.2015@live.rhul.ac.uk

Abstract

Dykes and inclined sheets are known occasionally to exploit faults as parts of their paths, but the conditions that allow this to happen are still not fully understood. In this paper, we report field observations from a swarm composed of 91 segments of dykes and inclined sheets, the swarm being particularly well-exposed in the mechanically layered caldera walls of the Santorini volcano, Greece. Here the focus is on dykes and sheets in the swarm that are seen deflected into faults and the mechanical conditions that encourage such deflections. In particular, we present new analytical and numerical models to explain the mechanical principles of dyke/sheet deflections into faults. The numerical models are applied to a normal-fault dipping 65° with a damage zone composed of parallel layers or zones of progressively more compliant rocks with increasing distance from the fault rupture plane. We model a sheet-intrusion, dipping from 0˚ to 90˚ and with an overpressure of alternatively 1 MPa and 5 MPa, approaching the fault. We further tested the effects of changing (1) the thickness of the sheet-intrusion, (2) the fault-zone thickness, (3) the fault-zone dip-dimension (height), and (4) the loading by, alternatively, regional tension and compression. We find that the stiffness of the fault core, where a compliant core characterises recently active fault zones, has pronounced effects on the orientation and magnitudes of the local stresses and, thereby, on the likelihood of dyke/sheet deflection into the fault zone. Similarly, the analytical models, focusing on the fault-zone tensile strength and energy conditions for dyke/sheet deflection, indicate that dykes/sheets are most likely to be deflected into and use steeply dipping recently active (zero tensile-strength) normal faults as parts of their paths.

KEYWORDS: dykes, inclined sheets, faults, dyke deflection, sheet deflection, analytical models, numerical models, Santorini Greece

1. Introduction

Propagation of dykes and inclined sheets is the most common form of magma transfer from shallow magma chambers to fissures feeding volcanic eruptions (e.g., Gudmundsson, 2020). Most dykes/sheets form their paths through the Earth's crust by rupturing the host rock and forming fluid-driven extensional fractures (e.g., Anderson, 1951; Rubin and Pollard, 1987; Rubin, 1995; Gudmundsson, 1986, 2020; Tibaldi, 1992, 2015; Saunders 2004). When forming their paths, dyke/sheets use existing joints that coincide with the direction of the maximum principal compressive stress σ_1 and are perpendicular to the minimum principal compressive stress, σ_3 (e.g., Anderson, 1951; Gudmundsson, 2011). However, stress changes during magma propagation associated with host rock heterogeneity (e.g., Gudmundsson 2020; Drymoni et al., 2020), seismic activity or ground deformation (e.g., Geyer and Gottsmann 2010; Bonali et al., 2013; Tibaldi et al., 2017; Kiryukhin et al., 2020) and many other factors (e.g., van Wyk de Vries and Matela 1998; Geyer and Gottsmann 2008; Delcamp et al., 2012; Magee et al., 2017) can alter the magma path towards the surface and the likelihood of an eruption (e.g., Roman et al., 2006; Neuberg et al., 2018). While most dykes/sheets form their own fractures, some follow pre-existing faults for parts of their propagation paths (e.g., Cembrano and Lara, 2009; Aloisi et al., 2011; Le Corvec et al. 2013, 2018; Spacapan et al., 2016; Dumont et al., 2016; Sielfeld et al., 2019; Gudmundsson, 2020). For an active fault, the rupture (fault) plane is oblique to σ_1 and σ_3, so that the parts of dykes/sheets that follow them are no longer pure extension fractures (mode I cracks) but rather shear cracks.

One model to explain the propagation paths of dykes and inclined sheets uses the concept of least action which, when the kinetic energy is insignificant, reduces to the principle of minimum potential energy (Gudmundsson, 1986, 2000). Then dykes/sheets propagate parallel with σ_1 (and perpendicular to σ_3) so long as that direction coincides with the direction of minimum tensile strength, T_o. In this model, a propagating dyke will at any time pick the most economical path (the path that requires least energy), either wholly or partly, and hence use normal, reverse or strike-slip faults of low or zero tensile strength (that is, recently active faults), when they are favourably oriented in relation to the local stress field during dyke emplacement. While field observations of the mechanical interactions between dyke and faults

are not very common, several examples of dykes occupying faults have been reported (Gudmundsson, 1983, 1986; Delaney, 1986; Rossetti et al., 2000; Mathieu et al., 2008; Spacapan et al., 2016). Similarly,-Browning and Gudmundsson (2015) observed the deflection of inclined sheets into a part of a normal fault bounding a caldera. However, as field observations are limited, so is our understanding of the mechanisms and conditions under which dykes/sheets utilise pre-existing faults for parts of their paths.

Santorini volcano, with its well-exposed caldera walls, is a natural laboratory that offers excellent opportunities for field observations of dyke propagation, dyke arrest, and dyke deflection into contacts and faults (Drymoni et al., 2020). The northern caldera wall, in particular, contains a local swarm of dykes, as well as many normal and strike-slip faults, all of which dissect heterogeneous and anisotropic host rock. Therefore, the northern caldera wall offers excellent opportunities for studying dyke-fault interactions and does, indeed, show several examples of dykes being deflected into faults.

The principal aim of this paper aims to address the conditions and mechanics that control magma ascent when a dyke or an inclined sheet meets an existing fault. More specifically, we aim at improved understanding as to how and under what conditions magma-filled fractures become deflected into an existing fault – thereby addressing the long-standing issue of the volcanotectonic relationship between faults and magmatism. We provide detailed field observations and analytical and numerical models which, that combined with real-time observations during unrest periods with dyke/sheet propagation, yield a framework for more reliable forecasting of the likely path of propagating dykes/sheets during unrest periods in volcanoes.

2. Mechanics of fracture initiation, growth, and propagation

Understanding of the mechanics of dyke/sheet propagation in the crust is essential for making reliable models towards forecasting volcanic eruptions. Fracture-mechanics concepts apply to all solids, including rocks at different scales. In the present study, the focus is on the outcrop scale, that is, the scale of fractures as seen in the field, which is the scale most relevant to volcanotectonics. Quantitatively, that scale covers the size range from tens of centimetres to tens of kilometres.

To address mechanical interactions between magma-filled fractures and faults it is essential to understand how fractures form and propagate and under which conditions a magma-filled fracture would prefer to follow a pre-existing shear fracture, a fault, rather than continue making its own extension-fracture path. Using results from fracture mechanics and materials science as to focus on the parameters that control the initiation, growth, and propagation of a magma-driven fracture and, in particular, deflection from its main path. Subsequently, we combine structural geology results and analytical and numerical modelling to give insights into the ways that a dyke/sheet acts mechanically on approaching a fault.

In the literature, the terms crack and fracture are often interchangeable. Here we follow the terminology of Broek (1982), where a fracture can be regarded as an extended crack. Furthermore, in modelling fractures, we use 'crack'; thus, we refer to Mode I, Mode II, and Mode III cracks, as is common in fracture mechanics literature (Gudmundsson, 2011).

The mechanics that govern fracture propagation in general, including the magma-driven fractures that generate dykes/sheets, was initially suggested by Griffith (1920, 1924). Accordingly, larger fractures develop from very small cracks or flaws (Griffith's theory was initially developed for fractures in glass), which for a propagating fault or a dyke/sheet fracture may be regarded as being located primarily in the process zone at the fracture/fault tip (Fig. 1; Atkinson, 1987; Atkinson and Meredith, 1987; Gudmundsson, 2011). These cracks are elliptical, thin, and, for many materials, atomically sharp, but for many rocks would be of dimensions similar to those of crystal boundaries and, on a larger scale, those of joints. If the stress that concentrates at the tip of already formed flaws equals the tensile strength of the host rock (Griffith's initial theory was for tension fractures, thus tensile strength), cracks grow and eventually coalesce to form a fracture which propagates along the process zone.

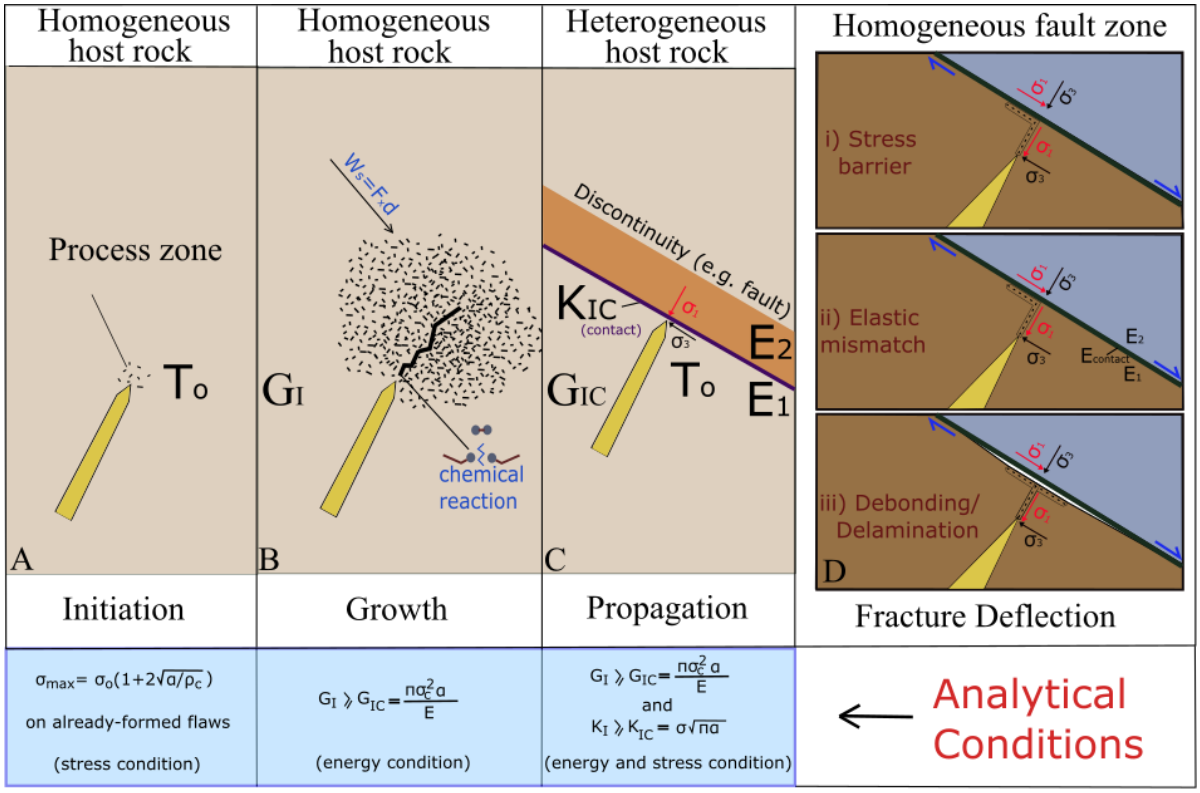

Fig. 1: Illustration showing the progressive formation of a Mode I crack, an extension fracture. A) Microcracks concentrate around the tip of a fracture in a linear elastic, brittle, material. Further crack nucleation and growth occurs within the process zone when the tensile stress at the tip of the fracture matches the tensile strength of the host rock. B) Crack growth is encouraged as the strain energy release rate (G_I) of the system rises. C) Crack propagation or fracture is controlled by the material properties of the host rock for any energy criteria used for the crack. D) Deflection mechanisms, i) stress barrier, ii) elastic mismatch and iii) debonding/delamination. All analytical fracture-mechanics solutions are from Broek (1982). W_S denotes the surface energy needed to produce a fracture, K_I is the stress intensity factor of a Mode I fracture, K_{IC} is the critical stress intensity factor or fracture toughness of a Mode I fracture, G_I is the strain energy of a Mode I fracture, the energy release rate of the material that controls the growth of the fracture, G_{IC} is the critical elastic strain energy or material toughness of a Mode I fracture, T_o is the tensile strength of the host rock, E is the Young's modulus (stiffness) of the host rock, σ_{max} is the maximum tensile stress at the tip of a semi-elliptical notch (the Griffith flaw/crack), α is the half length of a crack, σ_o is the remote tensile stress (due to loading such as magma-chamber expansion and crustal segment/volcano inflation), σ_c is the critical tensile stress, σ_1 is the maximum principal compressive stress and σ_3 is the minimum principal compressive stress or the tensile stress of the fracture, ρ_c is the radius of curvature. All these symbols, and others used in the paper, are further explained in Table 1.

Fracture initiation and growth requires brittle rocks to overcome the resistance to failure. Certain energy and stress conditions must be satisfied as they control the growth of cracks that eventually coalesce to form a large-scale propagating fracture. One measure of rock strength or toughness for Mode I fractures is the energy released rate G_I and the stress intensity factor K_I. The first is the energy per unit area of crack extension, and the second is the intensity of the stress field at the tip of the crack. A sufficient amount of elastic strain energy is required for a fracture to nucleate or grow (Fig. 1A&B). The strain energy is stored elastically in the body when the latter deforms – such as in a crustal segment, and associated volcano during inflation - and is released when the new fracture surface is generated. The amount of energy needed for crack growth is transferred into the system in the following ways (Broek, 1982; Gudmundsson, 2011):

1) Elastic strain energy (U_0) that is stored in the host rock, for example, during inflation, and can be used to rupture the rock.
2) The energy that enters the system due to work (W_L) done during displacement of, for example, the volcanic flanks or a part of a rift zone, when an inclined sheet or a dyke propagates within the crustal segment.
3) The surface energy (W_s) needed to generate two new surfaces as the crack develops in the rock body.
4) The total energy U_{tot} needed for the generation of new crack surfaces is the stored elastic strain energy (U_0) minus the work done on the system by displacements of the crack boundaries (subject to load control) (W_L) plus the surface energy or work (W_S), given by:

$$U_{tot} = (U_0 - W_L) + W_s \qquad (1)$$

The strain energy release rate, denoted by G_I (for Mode I cracks), determines the crack growth and is given by:

$$G_I = \frac{\sigma^2 \pi \alpha}{E} \qquad (2)$$

Where σ is the tensile stress, α is the half length of a crack and E the Young's modulus of the rock (or any other solid as the case may be).

The energy condition on its own does not govern fracture propagation, which is also related to the material properties and the stress conditions with the host rock. Specifically, at the propagation stage of fracture development, the fracture must overcome G_{IC} (material toughness) or K_{IC} (fracture toughness) for Mode I fractures which are connected as follows:

$$G_{IC} = \frac{{K_{IC}}^2}{E} \qquad (3)$$

The material toughness (G_{IC}) is a material constant which has the units of J m^{-2}; it indicates the energy required to rupture the rock, that is, the energy absorbed by the rock per unit area of the fracture. K_{IC} is the stress intensity factor or the fracture toughness of the rock and has the units of MPa m$^{1/2}$. If both G_{IC} and K_{IC} reach their minimum critical level, then a fracture can propagate (Fig. 1C). Laboratory measurements of material and fracture toughness for solid rocks are 20-400 J m^{-2} and 0.5-3 MPa m$^{1/2}$, respectively (e.g., Fourney, 1983; Atkinson and Meredith, 1987; Gudmundsson, 2011 and references therein).

Dyke propagation normally occurs parallel to the direction (or trajectory) of σ_1 and, therefore, perpendicular to σ_3 (e.g., Anderson 1951; Gudmundsson, 2020). Fracture propagation in heterogeneous crustal segments is primarily controlled by the difference in material properties between layers or by discontinuities between the layers, such as contacts or faults (Fig. 1C). The main mechanisms that control this process are 1) stress barriers, 2) elastic mismatch and, 3) debonding or delamination (He and Hutchinson, 1989; Hutchinson, 1996; Xu et al., 2003; Wang and Hu, 2006; Gudmundsson and Lotveit, 2012). These mechanisms control whether a fracture will propagate, deflect, or become arrested within the crustal segment (Fig. 1D).

3. Dyke-Deflection mechanisms

3.1 General overview

Inclined sheets and dykes are tabular, planar (primarily) extension fractures which form discordant to the host rock and dip from approximately 30˚ to 90˚. Inclined (cone) sheets and dykes are injected either from deep-seated reservoirs, which generally form sub-vertical dykes, or from shallow magma chambers, which can instead create sheets with various dips as well as sub-vertical dykes (Gudmundsson, 1999).

For a dyke that follows the direction of σ_1, and is thus perpendicular to σ_3, the dyke must deflect when the orientation of the principal stresses rotates ahead or at its tip (e.g., Anderson, 1936, 1951). On deflection, the dyke propagation path changes direction. The change may be permanent, such as when a dyke is deflected into a large sill or 'temporary' in the sense that a small part of the path of the dyke is deflected and thus different from the main path. (While 'temporary' as regards the actual propagation of the dyke, the deflection, of course, becomes permanent in the sense that the deflected part becomes 'frozen' with the rest of the path when the dyke solidifies.) Stress rotation is most likely to happen due to mechanical anisotropy (layering) in the crustal segment, particularly at a mechanical interface. Dyke deflection is primarily attributable to the following three mechanisms (cf. Gudmundsson, 2020).

1. Stress barrier: A stress barrier can be either a soft or a stiff layer that rotates the principal stress orientations and hence either stops or alters the propagation path of an extension fracture such as a dyke.
2. Elastic mismatch: Mismatch relates the Dundurs mismatch criteria or the difference in elastic properties (primarily Young's modulus) across a discontinuity or contact with the elastic properties of the contact itself. Great difference promotes deflection into the contact, particularly if the layer above the contact (in a vertical section) is much stiffer (with a higher Young's modulus) than the layer below the contact (and hosting the top part of the dyke as it approaches the contact).
3. Cook-Gordon debonding and delamination: Due to dyke-parallel tensile stress ahead of a propagating fracture tip, a weak (low tensile-strength) contact can debond and delaminate open) ahead of the dyke approaching dyke tip. On meeting the open contact, the dyke then either becomes deflected into a sill along the contact or, alternatively, stops altogether (becomes arrested).

3.2 Deflection of dykes into faults

Fault zones are Mode II or III (shear) fractures that may both encourage and inhibit fluid flow in the crust. They form mechanical, and displacement discontinuities called cores and damage zones-which can gradually grow (Caine, 1996). Two main hydromechanical units define the architecture of a fault:

1) a central fault core (commonly from a few centimetres to tens of meters thick), which accommodates the bulk of fault displacement, and

2) a brittle damage zone (from a few metres to several hundred meters or more in thickness) which is associated with the growth and evolution of fractures, veins, small faults or even folds, in the host rock (e.g., Chester and Logan 1986; Caine et al., 1996, Faulkner et al., 2010, 2011; Gudmundsson, 2011). Intrinsic mechanical properties, such as strength and stiffness, of a fault zone differ between the core and the damage zone. The fault core in an active fault is mostly composed of narrow slip surfaces (Caine et al., 1991), soft breccia and geochemically altered rocks, gouge and unconsolidated rocks (Anderson et al., 1983; Hoek 2000) which have commonly a very low Young's moduli (typically less than 1GPa) (Gudmundsson, 2011; Heap et al., 2020). The damage zone is characterised by fractures whose frequency is normally highest at the damage zone – core boundary and decreases (often in an irregular manner) from there to the damage zone contact with the host rock. It follows the stiffness of rocks in the damage zone gradate from relatively compliant (high fracture frequency) near the core to relatively stiff nearer the host rock or protolith. For an active fault, the core itself, has normally the lowest Young's and accommodates much of the fault-zone displacement. However, during periods of inactivity, the fault core can become locked and very stiff (with Young's moduli of higher than 10 GPa.

Table 1

List of parameters and variables

Variable	Definition	Units
α	half-length of a crack	m
α	angle between the fault plane and the direction of σ_1	degrees
δ	variational symbol	-
d	distance	m
E	Young's modulus (stiffness) of the rock	Pa
F	force	N
g	acceleration due to gravity	m s^2
h	dip-dimension of a dyke	m
G_I	strain energy release rate for a Mode I fracture	J m^{-2}
G_{IC}	critical elastic strain energy or material toughness of a Mode I fracture	J m^{-2}

K_I	stress intensity factor of a Mode I fracture	MPa $m^{1/2}$
K_{IC}	critical stress intensity factor or fracture toughness of a Mode I fracture	MPa $m^{1/2}$
Po	overpressure	Pa
$P_o^{\sigma n}$	overpressure needed for a dyke-fracture to open against σ_n	Pa
p_e	excess pressure	Pa
Π	total potential energy of a system	J
ρ_c	radius of curvature	m
ρ_m	magma density	kg m^{-3}
ρ_r	crustal density of the rock	kg m^{-3}
σ	tensile stress	Pa
σ_c	critical tensile stress	Pa
σ_d	differential stress	Pa
σ_{max}	maximum tensile stress at the tip of a semi-elliptical notch (the Griffith flaw/crack)	Pa
σ_n	normal stress	Pa
σ_o	remote tensile stress (due to loading such as magma-chamber expansion and crustal segment/volcano inflation)	Pa
σ_1	maximum principal compressive stress of the fracture	Pa
σ_3	minimum principal compressive stress or the tensile stress of the fracture	Pa
τ	shear stress	Pa

S	action	J s
T	kinetic energy of the system	J
T_o	tensile strength of the host rock	Pa
$T_o^{\sigma 3}$	tensile strength along the path that is perpendicular to σ_3	Pa
$T_o^{\sigma n}$	tensile strength along the path that is perpendicular to σ_n	Pa
t_1	arbitrary time	s
U_o	elastic strain energy	J
v	Poisson's ratio	-
W_L	work subject to load control	J
W_S	surface energy or work	J

The condition that defines whether a dyke will propagate through a pre-existing fracture, a fault, or will make its own path is mechanically defined by two parameters, namely:

1) The tensile strength (T_o) of the fault plane.

2) Hamilton's principle of least action, which means that the path followed by a system is the one that makes the action has an extremum, normally a minimum. Action has the units of energy × time, that is, J s (joule-second). For dyke propagation, the principle of least action can be stated, in its simplest form, so that the dyke/sheet selects the path along which the time integral of the difference between the kinetic and potential energies is an extremum, and normally a minimum, with reference to all other potential paths with the same points of initiation (at the magma chamber) and arrest (or eruption). For a continuous system, such as a crustal segment, the Hamilton's principle may be stated as follows (Gudmundsson 2020):

$$\delta S = \delta \int_{t1}^{t2} (T - \Pi) dt = 0 \qquad (4)$$

where Π is the total potential energy of the system, namely the sum of the total stored strain energy and the potential energy of the external forces acting on the rock body/crustal segment, T is the kinetic energy of the system, S is the action, δ is the variational symbol – denoting a small change – and t_1 and t_2 are two arbitrarily chosen times in the evolution of the system (here dyke/sheet propagation).

When the kinetic energy T is omitted (during the generally slow dyke propagation) and all the forces are conservative – as is common for elastic systems, then Hamilton's principle of least action (Eq. 4) reduces to the principle of minimum potential energy, which can be stated as follows (Gudmundsson, 2020):

$$\delta \Pi = 0 \qquad (5)$$

This principle states that of all possible displacement fields (during dyke propagation) that satisfy the constraints and the loads on the system (the crustal segment), the actual displacements are those that make the total potential energy of the rock body/crustal segment a minimum.

To identify the mechanical conditions that encourage a dyke to follow a fault partly or wholly we need to calculate the normal stress (σ_n) on the fault plane and the difference between this normal stress and the minimum principal compressive stress (σ_3). Both are defined by the following equations (Eqs. 6&7):

$$\sigma_n = \frac{\sigma_1 + \sigma_3}{2} - \frac{\sigma_1 - \sigma_3}{2} \cos 2\alpha \qquad (6)$$

$$\sigma_n - \sigma_3 = \frac{\sigma_d}{2}(1 - \cos 2\alpha) \qquad (7)$$

where $\sigma_d = \sigma_1 - \sigma_3$ and α is the angle between the fault plane and the direction of σ_1.

It can be shown (Gudmundsson, 2020) that a dyke will use an active fault as part of its path if the following conditions are satisfied:

$$\sigma_n - \sigma_3 \leq \Delta T_0 \qquad (8)$$

where

$$\Delta T_0 = T_0^{\sigma_3} - T_0^{\sigma_n} \quad (9)$$

is the difference between the tensile strength along the path that is perpendicular to σ_3 (parallel with σ_1) and the path that is perpendicular to the normal stress on the path, σ_n. If the tensile strength along the path perpendicular to σ_n is zero, then we have:

$$\Delta T_0 = T_0 \quad (10)$$

Likewise, the overpressure needed for a dyke-fracture to open against σ_n, which is greater than the one needed to open the dyke-fracture against σ_3 (unless $\sigma_n = \sigma_3$), is defined by:

$$P_o^{\sigma n} = p_e + (\rho_r - \rho_m)\, gh + \frac{\sigma_d}{2}(1 + \cos 2\alpha) \quad (11)$$

Here p_e is the magmatic (fluid) excess pressure in the source chamber at rupture and dyke injection, ρ_r is the crustal density of the rock between the chamber and the surface, ρ_m is the magma density, g is the acceleration due to gravity acceleration, and h is the dip-dimension of the dyke (cf. Table 1).

In this study, we explore the mechanical conditions under which fault zones act as barriers or, alternatively, as channels for propagating dykes. We investigate those conditions under which dykes become deflected and document the interactions between dykes and faults in the caldera wall of Santorini volcano. The integration between analytical and numerical modelling provides mechanical constraints on the behaviour of a dyke on approaching a fault – constraints that are then tested by field observations.

4. Methods

4.1 Field data

As a typical active stratovolcano, Santorini has experienced many eruptive cycles and at least four caldera collapse episodes (Druitt & Francaviglia 1992). The past Plinian or subplinian volcanic activity has formed a complex pile of stratigraphic horizons. The activity has included (1) two explosive cycles, (2) dyke-fed eruptions, (3) a double-magma chamber volcanic

plumbing system (e.g., Druitt et al., 1999; Browning et al., 2015), and (4) a distinct magmatic fingerprint in the Aegean arc e.g., primary and evolved magmas affected by high degrees of partial melting and decompression melting but low degrees of crustal contamination, mantle release of hydrous fluids derived from the subducted basaltic slab, and low aqueous to sediment melt ratios during magma generation (Francalanci and Zellmer 2019).

The study area exhibits numerous dyke segments (Fig. 2) hosted by highly heterogeneous rock primarily generated by the oldest composite stratocone, the Peristeria Volcano (530-430 ka). The following events include the first eruptive cycle (360-172 ka), the cinder cones of the Megalo and Kokkino Vouno (125-80 ka) and the Skaros shield and Therasia dome complex (70-22 ka). The Minoan eruption (3.6 ka) marked the last Plinian eruption. The associated caldera collapse has exposed the contacts, the stratigraphic layers, the dykes and the regional faults, allowing them to be examined.

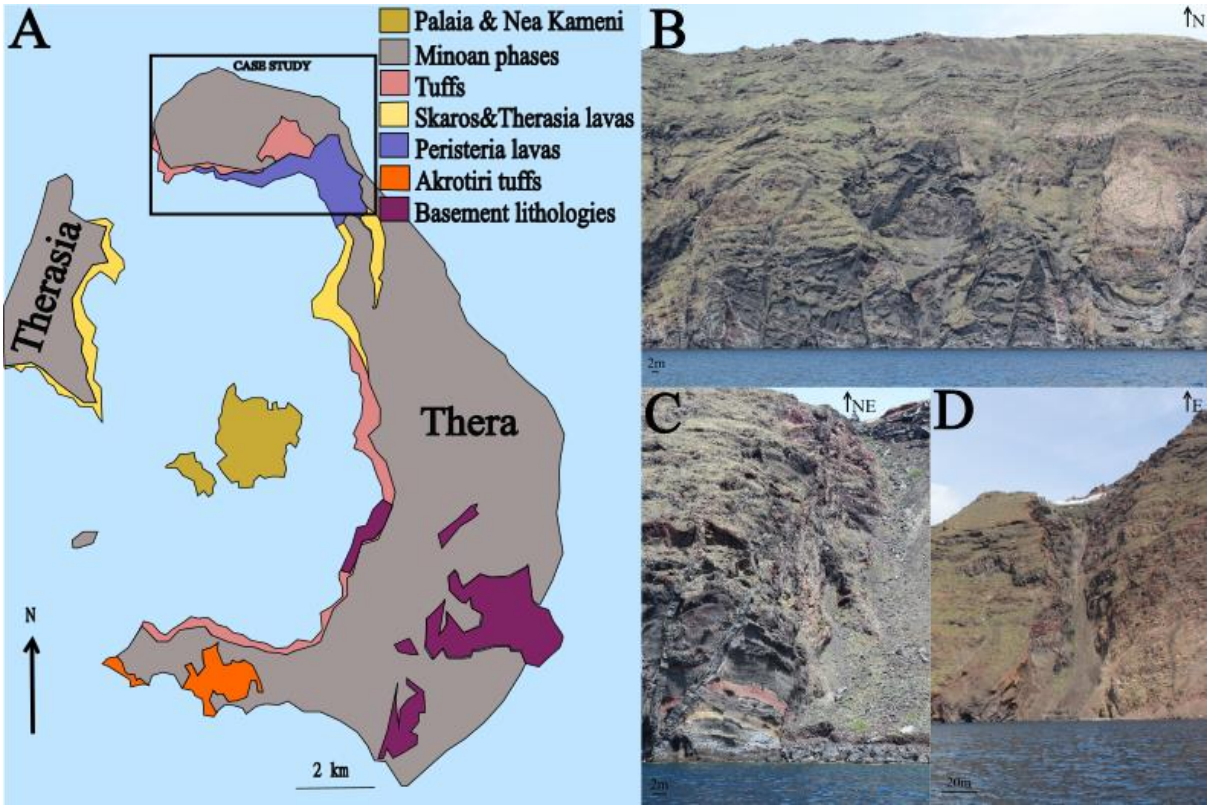

Fig 2: (A) Simplified geological map of Santorini (modified from Druitt et al., 1999). (B) Panorama of the northern caldera wall dyke swarm showing dyke segments that are not deflected into pre-existing faults. (C, D) Dyke-fault interactions in the outcrop scale.

We conducted field campaigns in the northern caldera wall and mapped the dyke segments, the associated host-rock layers, and fault zones (Figs. 2&3) (the structural analysis is presented in detail in Drymoni et al., 2020). We also studied the fault segments by collecting data on their

attitude and sense of slip. Several dykes were found to be deflected into the fault zones and were studied to investigate the factors controlling the deflection. Deflection was defined as an abrupt > 30° change in the dyke or sheet dip in a vertical (cliff) section. In this study, we particularly explore the interactions between the dyke, the inclined sheet, and the fault zone, as shown in Fig. 3. Both modelled intrusions are within a few metres of the fault zone (Fig. 3C). The field data was used as the geometrical and material parameters for analytical modelling and a suite of FEM numerical models using COMSOL Multiphysics.

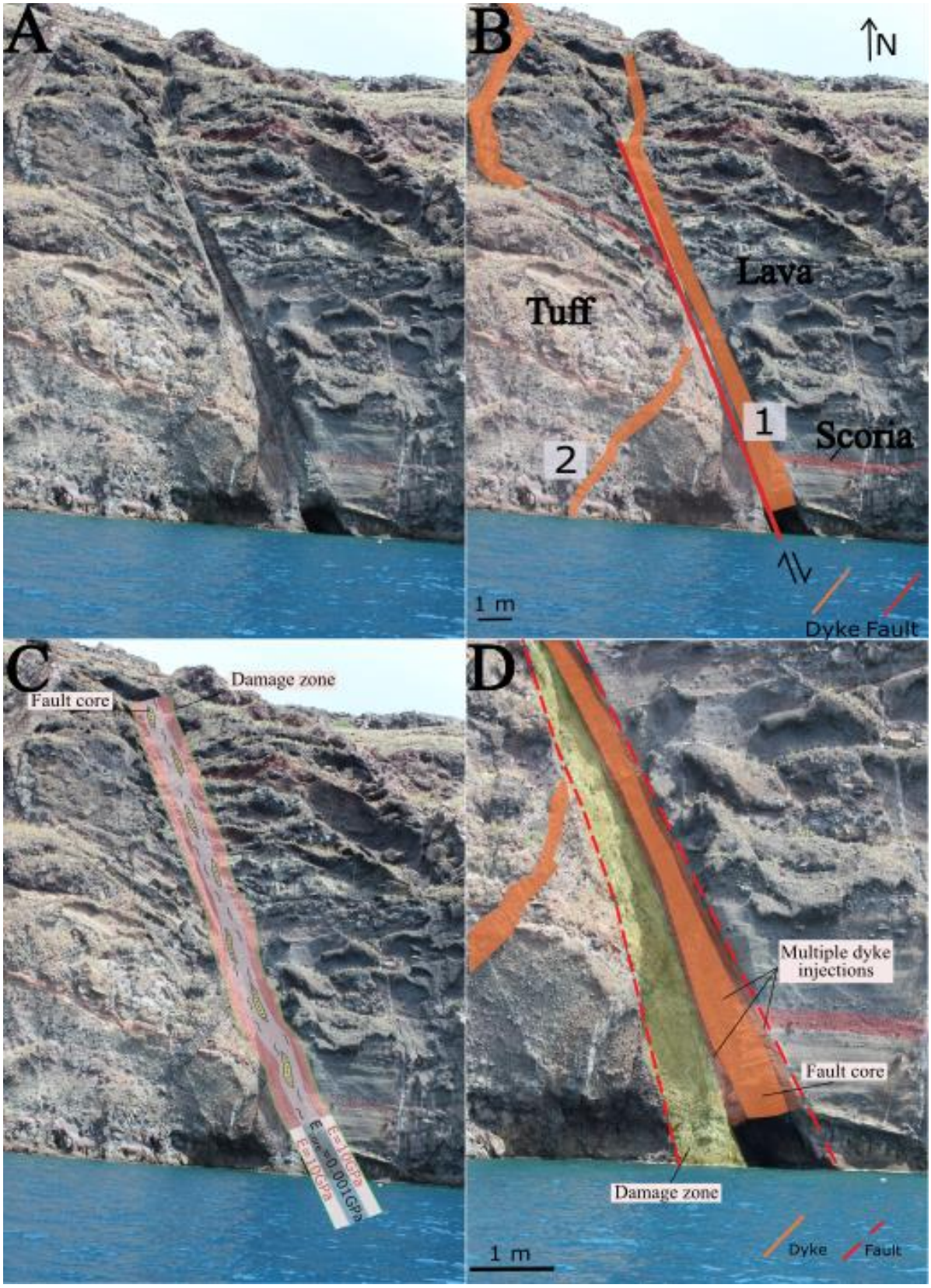

Fig. 3: Interactions between dykes and a normal fault zone. Original photo (Part A) and annotated photo (Part B). The numbers (1 and 2) indicate two sheet intrusions of different ages. One is a dyke (1) follows the fault and must have been deflected into it at greater depth. The

other (2) is an inclined sheet becomes that cures towards the fault zone and is parallel to it along part of its path (cf. Part D). Part C, close-up of the heterogeneous structure of the fault zone. (D) Close-up of the inclined sheet (2) where it is deflected into the fault zone and follows the damage zone.

4.2 Analytical model setup

We simulated a model setup (Fig. 4) where (1) a dyke was almost parallel to the fault dip (i.e. $D\theta$=0-10˚), (2) an inclined sheet with $D\theta$=65°, that is, the angle between fault and sheet being 65°, which is also the dip of the normal fault zone, as seen in the field. The dykes propagate parallel to σ_1 while the fault dip must be oblique to the maximum and minimum principal stresses during slip (when the fault is active). The shear stress (τ) is parallel to the dip of the fault plane, and the normal stress (σ_n) is perpendicular to the plane. In case the normal fault is recently active (had a recent fault slip), the tensile strength of the fault core is zero (Gudmundsson, 2020) in which case less energy may be needed for a dyke to follow the path of the fault than make its own fracture. When a dyke follows an active fault, the dyke propagates perpendicular to σ_n and not to σ_3.

Initially, we use Eqs. 6 and 7 to assess the likelihood of a dyke and the inclined sheet using the fault as a part of their paths, that is, to enter the fault. Then we calculate the overpressure needed for a dyke to open up against σ_n using Eq. 11. We determine analytically the mechanical conditions of the dyke emplacement (P_o, σ_d, P_e), as well as the angle between the fault and the dyke/sheet that would encourage a dyke to propagate into a pre-existing fault.

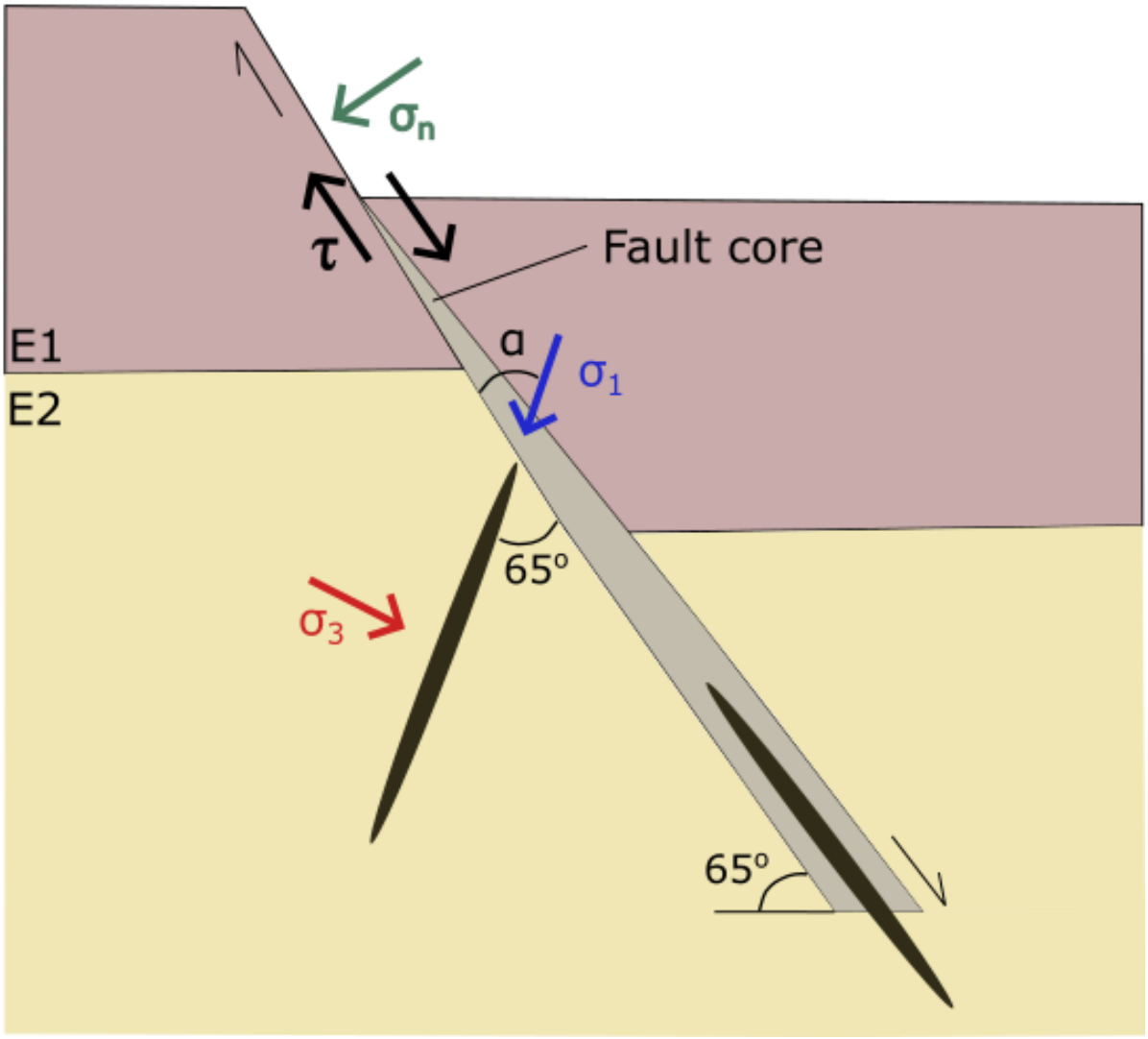

Fig. 4: A condition of dyke deflection between a normal fault and a dyke or an inclined sheet. Both sheet intrusions (black-filled ellipses) use the fault as a part of their paths and then continue to propagate through rupturing the rock and forming their own paths. σ_1 and σ_3 are the maximum and minimum principal compressive stresses, σ_n the normal stress, τ the shear stress, and α the angle between σ_1 and the fault plane. E1 and E2 denote two mechanically dissimilar layers.

4.3 Numerical model setups

We used the Finite Element Method (FEM) software COMSOL Multiphysics (v5.2) to simulate the observed interactions between dykes and faults in the northern caldera wall of Santorini. The basic geometry of the 2D plain strain models was derived from field observations, and a variety of boundary conditions were investigated to interpret the mechanisms that encouraged

412 the observed behaviours. In all the numerical models, the dykes were modelled as elliptical
413 cavities driven by overpressure (P_o). Although we tested different values (1 and 5 MPa), the
414 models presented here have 1 MPa magmatic overpressure, a representative value for the
415 Santorini boundary conditions during dyke emplacement (Drymoni et al., 2020). The resulting
416 thickness of the dyke depends on its overpressure (driving pressure), as is well known from
417 fracture mechanics (Gudmundsson, 2011), but for the overpressure used, the thickness is about
418 1 m. Also, the thickness of the fault zone is the same and equal to 1 m. In all models, the two-
419 dimensional area was bounded by an area with dimensions of 20 × 20 m. The models are linear
420 elastic, and the upper surface is a free surface, hence simulating the Earth's surface.
421
422 We explore the parameters that control the dyke-fault interactions partly through analysing the
423 effects of changing the stiffness or Young's modulus of both the host rocks and the fault zone
424 on the dyke-fault interaction. In the models, each fault zone is composed of three layers (e.g.,
425 Fig. 3C) that are symmetrically stratified in order to simulate a fault damage zone with
426 progressively increasing or decreasing fracture damage and Young's moduli (Gudmundsson,
427 2011; Ostermeijer et al., 2020). If the core of an active fault consists of gouge or breccia and/or
428 is highly fractured or pulverised, we assume a very low Young's modulus of 0.001 GPa (e.g.,
429 Heap et al., 2020) for the core. We assume that cores of inactive faults are much stiffer and
430 hence assign them Young's modulus of 10 GPa (Gudmundsson 2011). The Poisson's ratio for
431 the fault is 0.25 in all models (Heap et al., 2020). The fault plane dips 65° degrees, as observed
432 in the field and all its mechanical properties are isotropic.
433
434 We modelled the fault zone as (A) homogeneous, i.e. with the same mechanical properties
435 throughout but different to those of the host rock and (B) heterogeneous, i.e. with different
436 mechanical properties within the fault zone (Fig. 5). The dyke-fault interaction is modelled (a)
437 for a vertically propagating dyke meeting the fault and (b) for an inclined sheet meeting the
438 fault. We generated a very fine triangular COMSOL mesh which covered the whole modelled
439 area before the model runs. The mesh had a minimum element size equal to 0.0375 m-and a
440 curvature factor of 0.25. We fixed the modelled area of interest to be in the middle of the
441 assigned geometry to avoid edge effects. For the interpretation of the results, we plot the
442 magnitudes (contours) of minimum compressive (maximum tensile) principal stresses σ_3 as
443 well as the trajectories (directions, shown as arrows) of the maximum compressive principal
444 stress (σ_1) and the minimum compressive (maximum tensile) principal stress (σ_3) in all the
445 models.

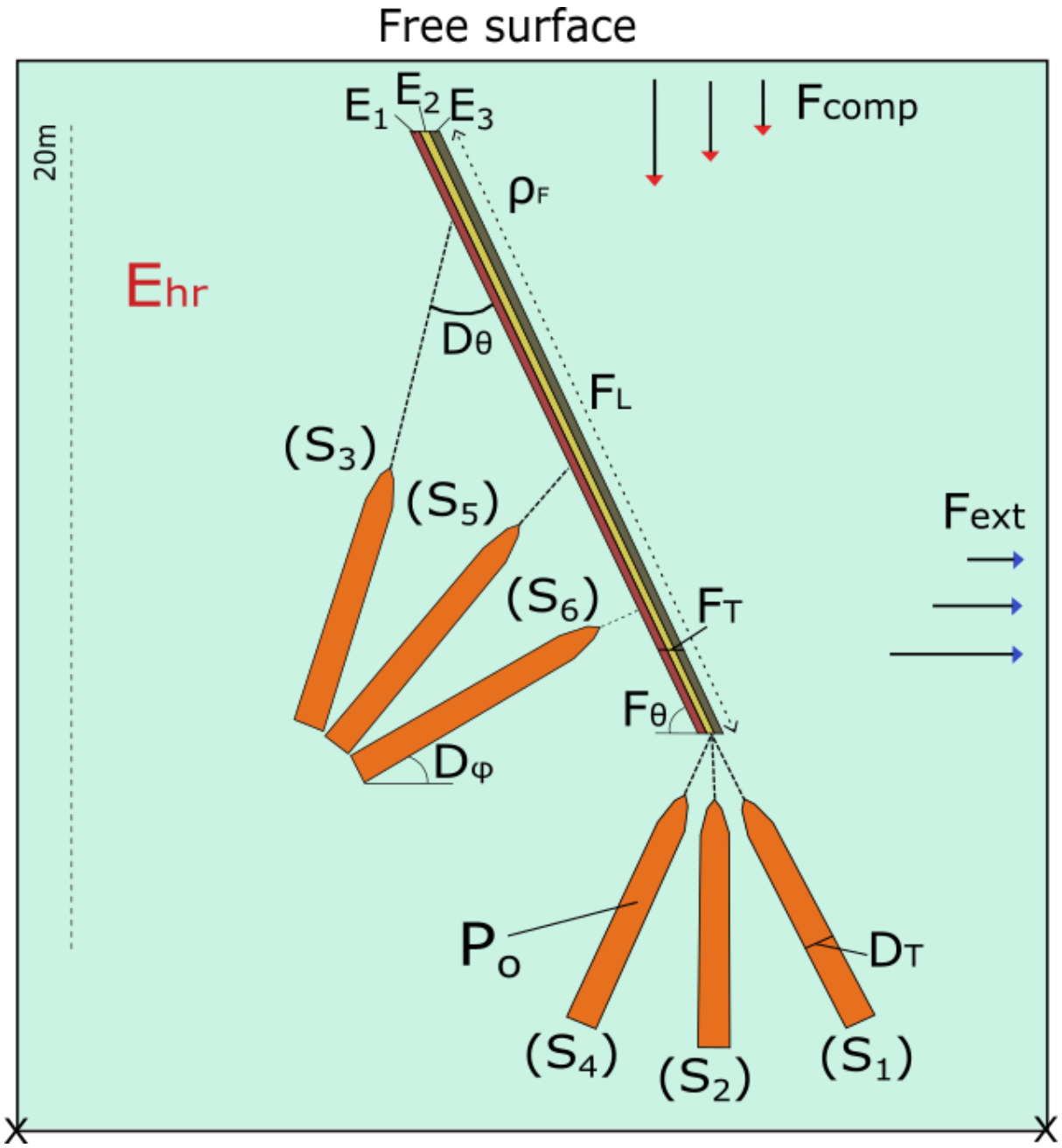

Fig. 5: Numerical model setups for a dyke (S1, S2, S4), and an inclined sheet (S3, S5, S6). The cavities (D_T) are with an internal pressure of 1 MPa (and 1 m opening). The normal fault has a thickness (F_T) of 1 m and a dip (F_θ) of 65 degrees and it is composed of three layers where both the Young's modulus of the core can be between 0.001 GPa to 10 GPa. The Young's modulus of the host rock (E_{hr}) is 40 GPa and the density of the fault (ρ_F) is 2000 kg/m^3. The minimum dip of the inclined sheet ($D\varphi$) is 50 degrees. For the sensitivity tests we use a varied Young's modulus for the fault (5 orders of magnitude 0.001-10 GPa) and a magmatic overpressure (P_o) of 1 MPa for the dyke. We modelled the angle of the dyke with the fault ($D\theta$) for 0˚ (S1), 25 (S2), 40˚ (S3), 50˚ (S4), 65˚ (S5) and 90˚ (S6), the thickness of the dyke for i) 1m (S7), ii) 3 m (S8), iii) 8m (S9), the thickness of the fault for i) 1 m (S10), ii) 5 m (S11), iii) 25 m (S12),

subject to an applied extensional stress field i) 0.5 MPa (S13), ii) 1 MPa (S14), iii) 3 MPa (S15), subject to an applied compressional stress field i) 0.5 MPa (S16), ii) 1 MPa (S17), iii) 3 MPa (S18), and a variant dip length of the fault zone i) 20 m (S19), ii) 100 m (S20), iii) 200 m (S21). The corners at the bottom of the model are fixed to prevent motion whereas the top corners are free. In the original models the elliptical cavities have thickness/length ratios of 100. S1-21 are the sensitivity tests as shown in Fig. 10.

4.4 Sensitivity tests model setups

The first case study models the influence of changing the angle of the dyke concerning the dip of the fault, and angle referred to as D_θ. Here the dip of the dyke and the inclined sheet was modified from 0-90° in steps, and the model re-ran each time. Then, we investigated the effect of changing the thickness of the dyke from 1 m to 3 m and then to 8 m and the thickness of the fault zone from 1 m to 2 m and finally to 25 m. We then modelled the dyke fault interaction subject to an applied tensile stress and compressive stress to the edges to replicate an extensional and a compressional stress field, respectively. For both scenarios, we assigned to the stress fields a variable σ_3 equal to 0.5, 1 and 3 MPa, values that could simulate the active stress field (Drymoni et al., 2020). The range of values used here (0.5-3 MPa) reflects common in situ tensile strengths and is also in harmony with the stress values used in modelling the stress field during the 2011-2012 unrest period (Feuillet 2013).

We also modelled different dip-lengths of the fault zone by adding either a 100 or 200 m high fault zone to the existing 20m observed fault zone. The fault was modelled subject to a wider range of Young's modulus values which are in specific five different orders of magnitude E1=0.001 GPa, E2= 0.01 GPa, E3=0.1 GPa, E4=1 GPa, E5=10 GPa showing a transition of a very active to an inactive fault core. Here we assigned a constant loading condition of magmatic overpressure (P_o) of 1 MPa as numerous models that designed but not presented here revealed that changes of loading conditions in that scale do not alter the stress field and hence the path of the dyke but only the magnitude of their stress concentration. The realistic model setups above, which were designed subject to the field observations, are shown in Figure 5.

5. Results

5.1 Field results

The field observations show that dyke 1 becomes deflected into the fault. Also, the inclined sheet becomes deflected into the fault but at a higher level (i.e., at a shallower crustal depth) in the succession (Fig. 3A). Both the dyke and the sheet were emplaced into the same heterogeneous and anisotropic host rock, which consists of lava flows, breccias, tuffs and scoria units. The dykes belong to the same population but either emplaced later or during the emplacement of the Peristeria or Skaros subswarms (Drymoni, 2020). The observed fault offset along the dip of the fault, as calculated from a scoria marker horizon, is approximately 6 m (Fig. 3).

5.2 Analytical model results

From Eqs. 7, 8 and 9 we assess the likelihood that the dyke and the inclined sheet would use the fault as part of their paths. Since the dip of the fault is 65˚, then the angle between the sheet-fault plane and σ1, α, is 90˚- 65˚= 25˚ and 0-10˚ for the dyke-fault plane, respectively. From Eq. 8 above and if the fault formed at 300 m depth (shallow crust), we use the values of σ_1 = 7.5 MPa and σ_3 =3.75 MPa, if at a depth 800 m below the surface of a rift zone the vertical stress is σ_1=20 MPa and σ_3=10 MPa (c.f. Gudmundsson 2020).

For the sheet-fault interaction we get the difference as:

$$\sigma_n - \sigma_3 = \frac{\sigma_d}{2}(1 - \cos 2\alpha) = \frac{7.5-3.75}{2}(1-\cos 50) = 0.6\ MPa \qquad (12)$$

For the dyke-fault interaction if the dyke meets the fault perpendicular to σ_n (α=0˚) we get the difference as:

$$\sigma_n - \sigma_3 = \frac{\sigma_d}{2}(1 - \cos 2\alpha) = \frac{7.5-3.75}{2}(1-\cos 0) = 0\ MPa \qquad (13)$$

For the dyke-fault interaction if the dyke meets the fault inclined to σ_n (α=10˚) we get the difference as:

$$\sigma_n - \sigma_3 = \frac{\sigma_d}{2}(1 - \cos 2\alpha) = \frac{7.5-3.75}{2}(1-\cos 20) = 0.1\ MPa \qquad (14)$$

From Eqs. 8 and 10 we have:

For the inclined sheet:

$$0.6 \leq \Delta T_o \qquad (15)$$

For the dyke:

$$0.1 \leq \Delta T_o \qquad (16)$$

The range for in-situ tensile strengths outside active faults is 0.5-9 MPa (Amadei and Stephansson, 1997; Gudmundsson, 2011) and most commonly 2-4 MPa. So, our calculated cases of 0.6 and 0.1 MPa for the amount of tensile stress is around the lower range of common tensile strengths. This suggests that the dyke and inclined sheet would likely only use the faults if they were active or recently active and hence with low tensile strengths within their core zone. This is in agreement with the field observations.

In a second stage, we use Eq. 11 to calculate the overpressure required for the dyke and the inclined sheet to open against σ_3. If we use the same values as previously, i.e., σ_d = 3.75 MPa, α=25˚, g=9.81 m s $^{-2}$, h= 300 m, and the excess pressure from the same shallow magma chamber is 1 MPa. We use the same magma density for both dykes since they are both

mafic and so ρ_m = 2650 kg m^{-3} and the average density of the layers above the roof of the shallow chamber is ρ_r = 2800 kg m^{-3}. This gives:

$$P_o^{\sigma n} = p_e + (\rho_r - \rho_m)\, gh + \frac{\sigma_d}{2}(1 + \cos 2a) = 1 \times 10^6 + (2800\text{-}2650) \times 9.81 \times 3 \times 10^2 + 0.6 \times 10^6$$

$$= 4.5 \text{ MPa} \quad (17)$$

Whereas in case the dyke was emplaced vertically into the host rock and made its own path, Eq. 11 would become:

$$P_o^{\sigma 3} = p_e + (\rho_r - \rho_m)\, gh + \sigma_d = 1 \times 10^6 + (2800\text{-}2650) \times 9.81 \times 3 \times 10^2 + 3.75 \times 10^6 = 5.1 \text{ MPa} \quad (18)$$

This then allows us to analytically determine the mechanical conditions of the emplacement in terms of dyke deflection or propagation. The results have shown that both fractures require less

554 overpressure to propagate through a fault zone rather than to make their own path if the fault
555 core has low tensile strength (T_o).
556
557 Finally, if we solve the inequality (Eqs. 8, 10) for the angle α (between σ_n and σ_1) and θ
558 (dyke/sheet-fault angle) we find:
559
560 $$cos\ 2\alpha \geq \left|\frac{2To}{\sigma_d} - 1\right| \qquad (19)$$
561
562 if $\sigma_d = 3.75$ MPa and T_o = 0.5-4 MPa for the range of typical rock tensile strengths we have:
563 - *For T_o=0.5 MPa then cos 2a ≥ |0.73|, cos 2a ≥cos 43˚, a≥22˚ and θ≥65˚*
564 - *For T_o=1 MPa then cos 2a ≥ |0.47|, cos 2a ≥ cos 62˚, a≥31˚ and θ≥59˚*
565 - *For T_o=1.5 MPa then cos 2a ≥ |0.2|, cos 2a ≥ cos 78˚, a≥39˚ and θ≥51˚*
566 - *For T_o=2 MPa then cos 2a ≥ |0.06|, cos 2a ≥ cos 87˚, a≥44˚ and θ≥46˚*
567 - *For T_o=2.5 MPa then cos 2a ≥ |0.3|, cos 2a ≥ cos 72˚, a≥36˚ and θ≥54˚*
568 - *For T_o=3 MPa then cos 2a ≥ |0.6|, cos 2a ≥ cos 53˚, a≥27˚ and θ≥63˚*
569 - *For T_o=3.5 MPa cos 2a ≥ |0.86|, cos 2a ≥ cos 30˚, a≥15˚ and θ≥75˚*
570 - *For T_o=4 MPa then cos 2a ≥ |0.92|, cos 2a ≥ cos 23˚, a≥12˚ and θ≥78˚*

571 The deflection threshold for the specific mechanical properties is shown in Fig. 6.
572

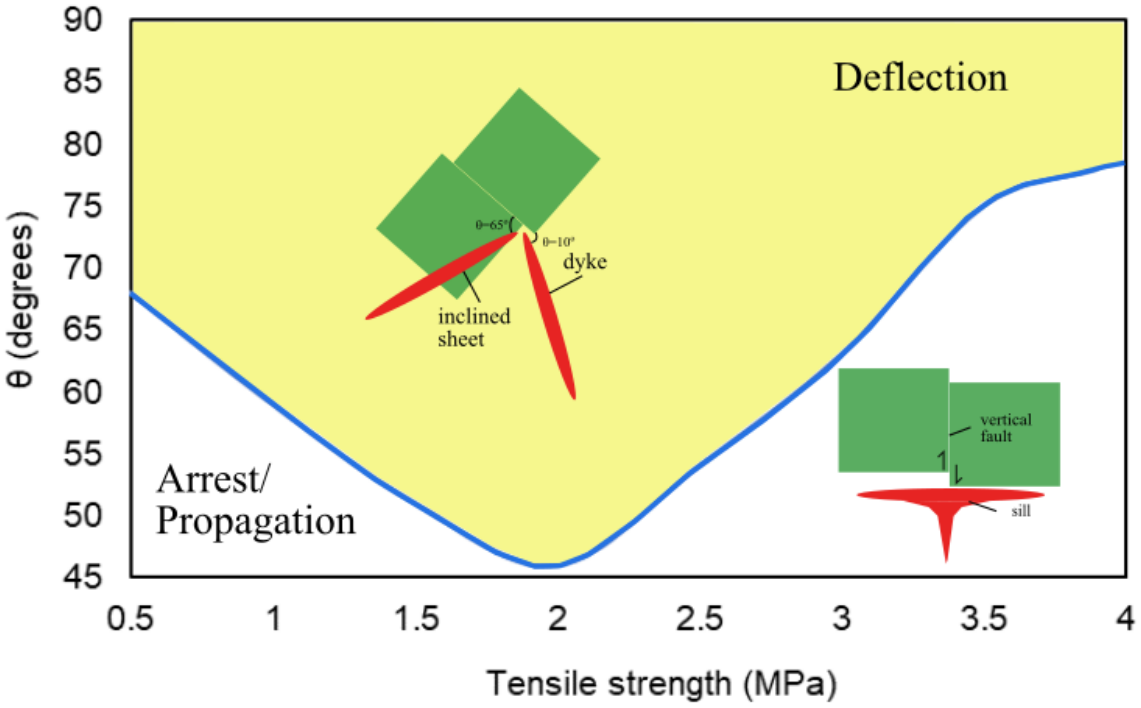

573

Fig. 6: Schematic diagram showing the analytical results of possible dyke or inclined sheet deflection/arrest at a fault by considering the tensile strength, along the fault plane and perpendicular to σ_3, and the dyke-fault angle is denoted as θ.

5.3 Numerical model results

The primary goal was to replicate the field observations with numerical models and hence explore the conditions that encouraged the deflection of the sheet intrusions and trace the relative order of emplacement sequence. Firstly, we modelled the interaction of both the dyke and the inclined sheet (Fig. 3) with a normal fault dipping 65˚and comprised of either a homogeneous or heterogeneous fault zone. We kept a constant thickness of 1m for both dykes. The dip length of the fault in the preliminary models is 20 m, but in later sensitivity tests, we also modelled fault zone dip lengths of between 20 and 200 m.

5.3.1 Homogeneous fault zone

In Figure 5 we see the results from a suite of models which simulated a homogeneous fault zone, i.e. one which has the same level of Young's modulus (1 GPa) throughout the fault. The vertical dyke (S2) and the inclined sheet (S6 were modelled in separate model setups, and both were assigned magmatic overpressures of 1 MPa. The host rock in both models had a Young's modulus of 40 GPa. We first modelled a homogeneous soft fault zone (0.001 GPa) and then a stiff zone (10 GPa). The model results are summarised as follows:

a) **E_{fault} = 0.001GPa (soft)**

In Figure 7A we show the results assuming a vertical dyke, and in Figure 7B an inclined sheet. First, we consider the results from the vertical dyke. The dyke is modelled at the apex of deepest part of the fault zone. The result is that the tensile stresses formed by the dyke overpressure are essentially symmetrical at the dyke tip with little perturbation caused by the fault. Further along the dip of the fault, to shallower levels, we note two contrasting trajectories or orientations of σ_1. To the left of the fault, the footwall in the natural case, the trajectories are aligned parallel with the fault dip, whereas to the right of the fault, the hanging wall in the natural case, the trajectories are either perpendicular to the fault or vertical. Furthermore, at the tip of the dyke

606 there is a rotation of the stress trajectories. This implies that the dyke would likely become
607 deflected and continue its path at an angle parallel to the fault zone.

608

609 In the case of the inclined sheet, which dips NW, or to the lower left in the models, and hence
610 creates an angle between the sheet and the fault (D_θ) of 50° (Fig. 7B), the stress distribution
611 (concentration) is more asymmetrical. There is a larger amount of tensile stress generated
612 beneath the dyke along the fault plane rather than above the dyke along the fault plane. The
613 stress trajectories in front of the inclined sheet do not rotate and remain parallel to the sheet.
614 This implies that the sheet would continue to propagate through the fault with a path of similar
615 dip to previously.

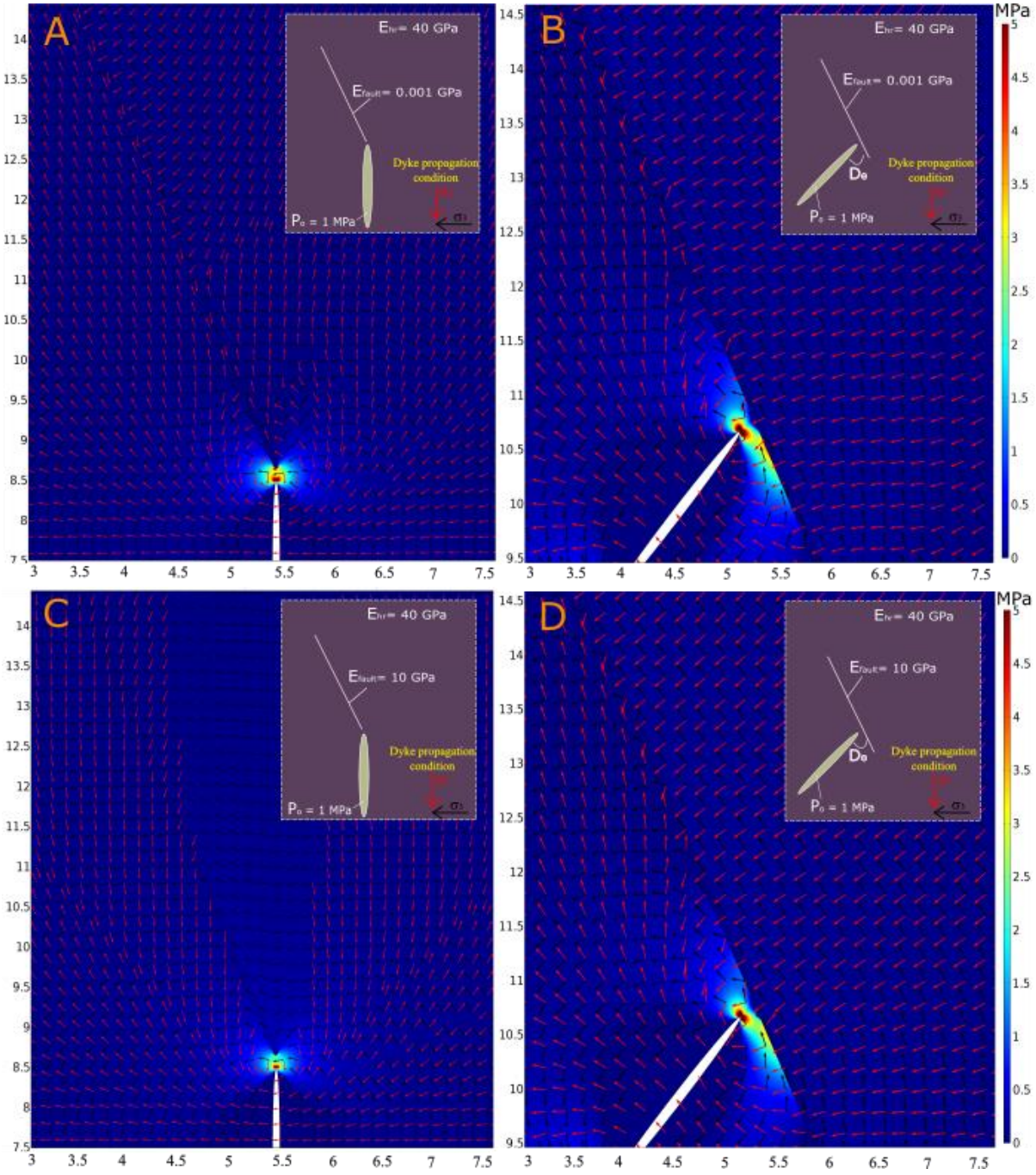

Fig. 7: FEM models of the distribution of tensile stress (σ_3), trajectories of maximum principal compressive stress (σ_1, red arrows) and the minimum principal stress (σ_3, black arrows) in the two geometries of fault-dyke interaction. Part A) a vertical dyke emplaced at the deepest part of a homogeneous fault zone of width 1 m and a soft fault core (E_{fault}=0.001 GPa). Part B) An inclined sheet with a length of 7m that makes an angle to the fault zone of D_θ is 50°; the fault zone is soft (E_{fault}=0.001 GPa). Part C) a vertical dyke emplaced at the deepest part of a homogeneous fault zone of width 1 m with a stiff fault core (E_{fault}=10 GPa). Part D) An inclined sheet with a dip of 7m that makes an angle to the homogeneous fault zone of D_θ is 50°; the

fault zone is stiff (E_{fault}=10 GPa). The host rock ($E_{hr)}$ has a Young's moduli of 40 GPa. The overpressure in both the dyke and the sheet is 1 MPa. y and x axis are in meters.

b) E_{fault} = 10GPa (stiff)

In the next stage, we assigned to the homogeneous normal fault a high Young's modulus value (E_{fault}=10 GPa) to investigate the dyke-fault deflection scenarios if the fault core was stiff. We observe that the stress distribution (concentration) ahead of the dyke tips for both the dyke and the inclined sheet are similar to the previous models (Fig, 7A and B). In the first model (Figure 7C), the trajectories of σ_1 are constantly vertical on both sides of the fault. However, in the second case (Figure 7D), the trajectories of σ_1 are more variable along the fault. To the left of the uppermost part of the fault the principal stresses are variable in orientation, whereas to the right of the fault σ_1 remains vertically oriented with respect to the fault plane. Also, the tensile stresses generated around the tips do not pass through the fault which results in the hanging wall part of the fault having a relatively lower amount of stress than the footwall. Both principal stresses (σ_1 and σ_3) at the tips were not rotated so dyke deflection would be unlikely. Instead, dyke propagation would occur parallel to σ_1, in this vertical, and the fault does not influence the magma path.

5.3.2 Heterogeneous fault zone

In the next set of models, we simulate a heterogeneous fault zone that dips 65° to the west and is composed of parallel layers of different stiffnesses. This setup is used to simulate a common fault zone architecture, i.e. one with a very soft fault core and a stiffer damage zone and conversely another with a stiff fault core and a softer fault damage zone. First, we examine the results where the fault core is filled with soft material such as gouge or clay and has a Young's modulus of 0.001 GPa.

c) $E_{fault\ core}$= 0.001GPa (soft fault core)

In Figure 8 we model a heterogeneous fault zone, i.e. of the fault contains units of different Young's moduli. In the first set of models, we assigned the fault core (E_{core}=0.001 GPa) to be soft in comparison to the outer fault zone (E_{rim}=10 GPa).

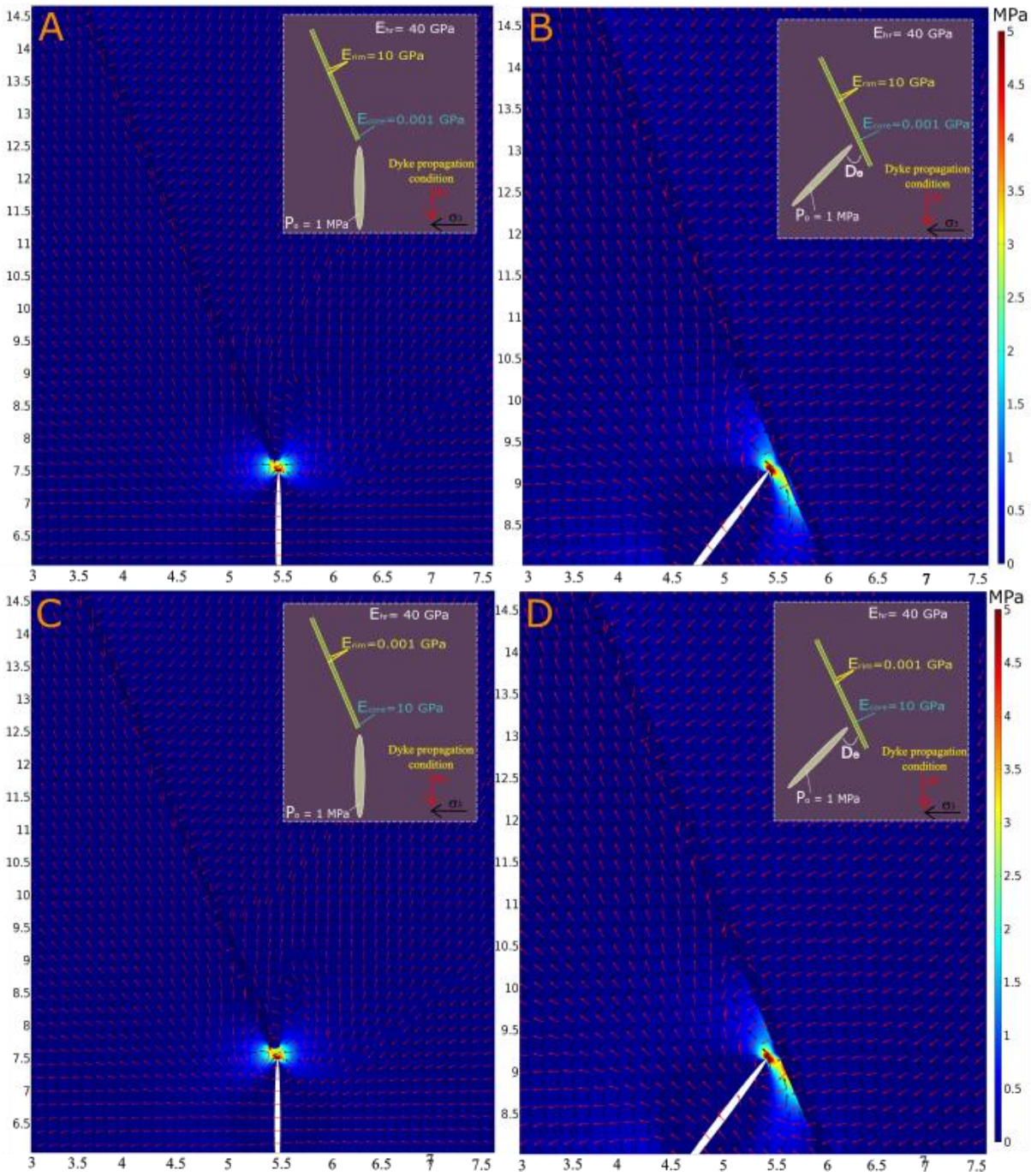

Fig. 8: FEM models of the distribution of tensile stress (σ_3) and trajectories of maximum principal compressive stress (σ_1, red arrows) and the minimum principal stress (σ_3, black arrows) in two geometries of fault-dyke interaction. Part (A) a vertical dyke emplaced at the deepest part of a heterogeneous fault zone of width 1 m and a soft fault core (E_{fault}=0.001 GPa). Part (B) An inclined sheet with a dip of 7m that makes an angle to the fault zone of D_θ is 50°;

667 the fault zone is heterogeneous and has a soft core (E_{fault}=0.001 GPa). Part (C) a vertical dyke
668 emplaced at the deepest part of a heterogeneous fault zone of width 1 m and a stiff fault core
669 (E_{fault}=10 GPa). Part (D) An inclined sheet with a dip of 7m that makes an angle to the fault
670 zone of D_θ is 50°; the fault zone is heterogeneous and has a stiff core (E_{fault}=10 GPa). The host
671 rock (E_{hr}) has a Young's moduli of 40 GPa. The overpressure in both the dyke and the sheet is
672 1 MPa. y and x axis are in meters.
673
674 We observe that the stress distribution (concentration) around the vertical dyke is symmetrical
675 while that around the inclined sheet is asymmetrical with higher concentrations at the lower
676 part of the fault. The trajectories of σ_1 in the lower part of the fault in Figure 8A are fault
677 parallel. However, on approaching the surface, the right fault wall shows stress rotations. In
678 Figure 8B, at the bottom part of the fault, σ_1 is perpendicular to the fault plane at the right side
679 and slightly rotated or parallel with the fault plane at the left on approaching the surface. Both
680 principal stresses (σ_1 and σ_3) in Figure 8A show a 90° rotation at the tip promoting dyke
681 deflection into the fault. In the inclined sheet model run, the principal stresses at the front of
682 the inclined sheet (Figure 8B) show an almost 90° maximum rotation; hence the inclined sheet
683 run promotes possibly deflection. In that case, the dyke will propagate through the stiff damage
684 zone and deflect parallel to the soft fault core and the inclined sheet will deflect as well higher
685 at the succession as shown in the field.
686
687 **d) $E_{fault\ core}$= 10GPa (stiff fault core)**
688
689 In Figure 8C and D, we show the results of a new suite of model runs. Here, the fault core has
690 a high Young's modulus (is stiff) of E=10 GPa and a low Young's modulus (soft) damage
691 zone. We observe similar stresses as in the previous case studies both for the vertical dyke and
692 the inclined sheet. In Figure 8C, the σ_1 trajectories are parallel to the fault plane at the right
693 side (hanging wall), while in the case of the inclined sheet the trajectories remain vertical to
694 the fault plane all over the heterogeneous fault zone close at its tip. Both principal stresses (σ_1
695 and σ_3) in Fig. 8C show a 90° rotation at the tip promoting dyke deflection into the soft margins
696 (edge of the damage zone). In the inclined sheet model run, the principal stresses at the front
697 of the sheet in Fig. 8D show a 45° maximum rotation; hence the inclined sheet run promotes
698 likely deflection into the soft margins (edge of the damage zone).
699

Generally, the sheet-intrusion stresses concentrate at the sheet tips whereas the fault-zone stresses concentrate at both around their tips as well as in their lower (bottom) parts. In addition, higher stresses are observed when the fault is stiff rather than soft. We observed that in a homogeneous fault zone the stress rotations were subject to the mechanical properties of the fault (Young's modulus) and the stresses for the vertical dyke could rotate when the fault is active (soft). The inclined sheet could not deflect under this scenario.

In a heterogeneous fault zone, the stress rotations were subject to the mechanical properties of the fault core and the fault margins (edge of the damage zone). When the fault core was soft, a stress barrier condition was completed, and both the vertical dyke and the inclined sheet are seen to become deflected and propagate parallel to it in this order. However, when the fault core was stiff, we observe no stress rotations at the dyke tip and neither the dyke nor the inclined sheet becomes deflected into the fault (Fig. 9).

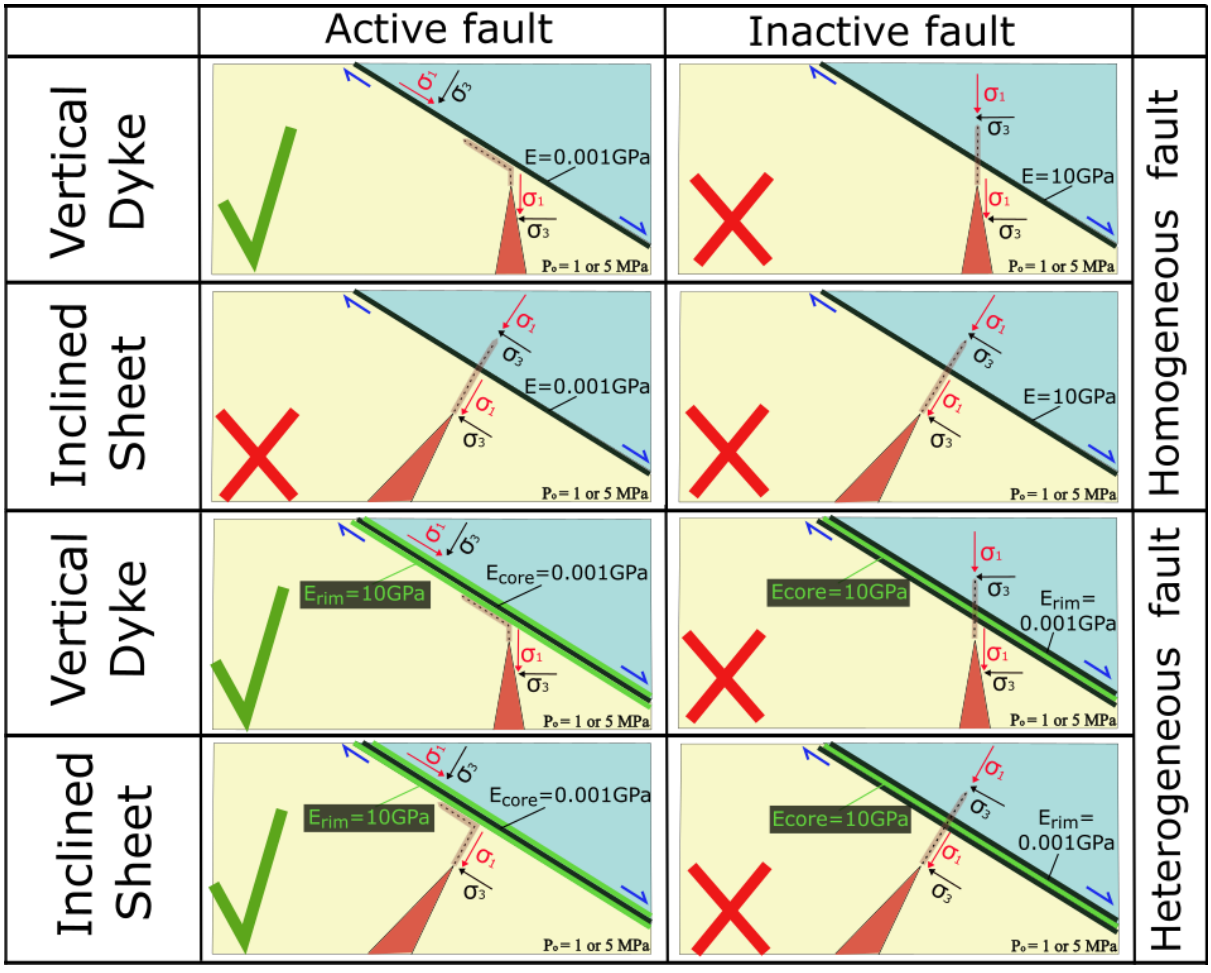

Fig. 9: Illustration showing the results of the FEM models. We observed that regardless the range of the magmatic overpressure (P_o) for both the vertical dyke and the inclined sheet, deflection occurs when the homogeneous fault is active (i.e with a low Young's modulus core)

rather than inactive (i.e. with a high Young's modulus core). In a homogeneous fault zone only, a vertical dyke can become deflected into the active fault. In a heterogeneous fault zone both the vertical dyke and the inclined sheet can be deflected into cores of the fault if they are sufficiently compliant. The green ticks indicate deflection, and the red crosses indicate propagation. The blue arrows indicate the fault kinematics seen in the field.

5.3.3 Sensitivity test results

We conducted a variety of sensitivity tests to investigate how specific parameters related to Santorini volcano could affect dyke-fault deflection in the shallow crust. We gave specific interest to the following parameters: (a) dyke-fault angle, (b) dyke thickness, (c) fault thickness, (d) extensional stress field, (e) compressional stress field, and (f) fault (dip) height.

It is evident that the stiffness of the fault is the main control and that of all of the other tested parameters only the dyke-fault angle and the fault thickness influence deflection mechanisms when compared with the fault zone stiffness. The results are summarized in Figure 10.

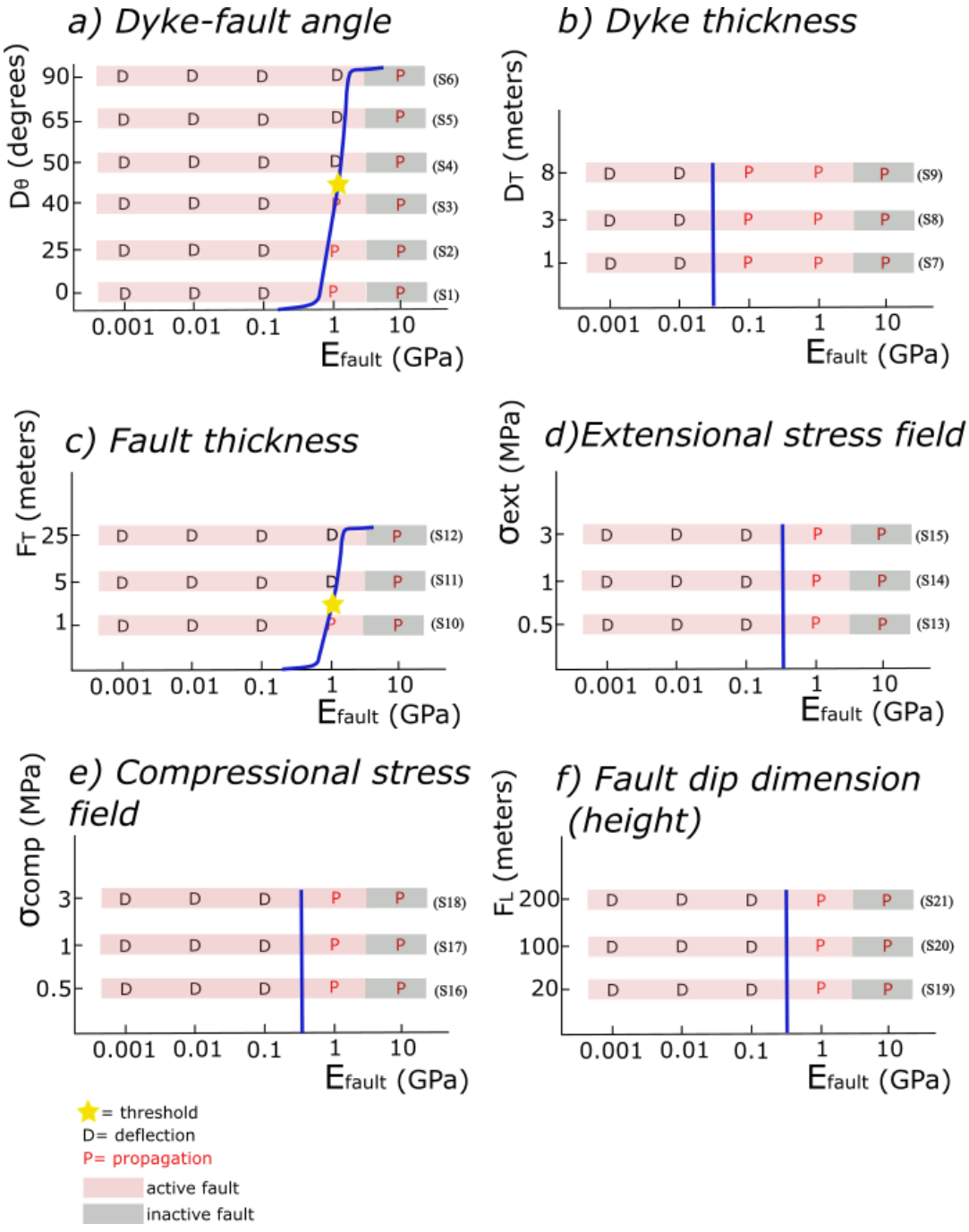

Fig. 10: Conditions that encourage dyke deflection (D) and dyke propagation (P) in a series of dyke and fault interactions associated with the angle of the dyke to the fault (a) (models S1-S6), the dyke thickness (b) (models S7-S9), the fault thickness (c) (models S10-S12), regional extension (d) (models S13-15), regional compression (e) (models S16-S18), and the fault height (f) (models S19-S21) in relation to the mechanical properties of a homogeneous fault zone. The models show that all parameters depend primarily on the stiffness of the fault core.

However, the dyke-fault angle and fault thickness can also promote dyke deflection in a relative stiff core (recently inactive) in case $D_\theta \geq 50^\circ$ and $F_T \geq 5$m.

6. Discussion

6.1 Synthesis of analytical results

The results from the analytical study suggest the following:

1. When the difference between the normal stress (σ_n) and the minimum principal compressive stress (σ_3) (Eq. 8) in fault zones small, both vertical dykes and inclined sheets can become deflected into faults. These theoretical results are supported by the field observations reported here (Fig. 3).
2. The calculated overpressures (Eqs. 17 & 18) required for a dyke or an inclined sheet to deflect into a fault rather than make its own path suggest that the condition $P_o^{\sigma n} < P_o^{\sigma 3}$ is commonly satisfied. This result implies that dykes and inclined sheets in our field area should tend to deflect into the fault, since using the fault requires lower overpressures.
3. The derived inequality (Eq. 19) suggests that if the fault zone has a low tensile strength (< 2 MPa) then a sheet-intrusion will become deflected into the fault if the angle between the sheet and fault is greater than 50˚.

6.2 Synthesis of numerical results

In the combined numerical study and sensitivity tests we made the following findings:

6.2.1 Effect of angle between faults and dykes/inclined sheets (D_θ)

Most of the dykes within the caldera wall dip subvertical, but there are eight inclined sheets with dips of between 50˚ and 70°. Most of the faults in the caldera wall dip 60˚-90˚. The attitude of dykes, inclined sheets, and faults influence the way that they interact. We investigated the influence of changing the angle (D_θ) with which a dyke or inclined sheet approaches a fault. We modelled the angles 0˚ (i.e. with the same dip), 25˚, 40˚, 50˚, 65˚ and 90˚ (i.e. when the dyke or inclined sheet meets perpendicular to a fault) (Fig. 5). The angle can be modified by changing either the fault angle or the inclined sheet angle. However, in our models, we keep the fault angle constant and change the dip of the inclined sheets.

We tested the effect of D_θ using variable values of fault stiffness ranging over five orders of magnitude and observed that deflection is always encouraged when the fault is compliant (E<1 GPa), regardless of the angle D_θ. However, when the fault core is stiffer and D_θ is 0˚- 50˚ (S1-S4), i.e. shallow, the dyke does not become deflected into the fault but instead permeates the fault. When D_θ is more than 50˚ (S5 and S6) and closer to vertical, the dykes show a tendency to deflect when the fault core is relatively soft (E=1 GPa) but not when it is very stiff (E=10 GPa) (Fig. 10a). The results are also in agreement with the first suite of numerical models reporting that the more vertical a dyke is when it meets an active fault, the easier it becomes deflected. The deflection threshold is hence $D_\theta \geq 50°$ and E≥1 GPa.

6.2.2 Effect of dyke thickness (D_T) and fault thickness (F_T)

We modelled the effect of dyke thicknesses (D_T) using the minimum (1m), maximum (8m) and average (3 m) thickness of dykes measured in the field. Generally, the more mafic dykes possessed thicknesses up to 3m, while a few felsic dykes were found to be as thick as 8m (Drymoni et al., 2020). The study of thickness variations then allows an approximate examination of the mechanical effect of different magma compositions on fault interactions. It is well known that the thickness of the dyke and inclined sheet is related to magma overpressure (Sneddon 1946; Gudmundsson, 2011; Geshi et al., 2020) so to investigate this parameter we tested the corresponding realistic values (Drymoni et al., 2020).

The results showed that dyke deflection is encouraged in very compliant fault zones (E<0.1 GPa) regardless of the dyke thickness (S7-S9). Similarly, these sensitivity tests can give us insights into whether the composition of the magma could be a parameter that could affect the mechanisms of dyke propagation. Our models suggest that dyke thickness is not a primary influence on dyke-fault interactions and certainly of lesser importance than the mechanical properties of the fault and the host rock (Fig. 10b). However, more parameters should be tested through numerical modelling, such as the rheology and viscosity of the magma. Our current study focused on the realistic outcrop parameters identified in the field able to promote deflection but not on the magmatic parameters, a task which is part of our future research agenda.

We also tested the influence of the fault zone thickness (F_T). We estimated that the faults zones (15 in total) within the Santorini northern caldera wall range from a few meters to about 25 metres thick (Drymoni 2020). We modelled the dyke-fault interaction by assigning a range of fault thickness values (1, 5 and 25 m) based on the field observations (S10-S12). Our results showed that, regardless of their thickness, soft fault zones are always more likely to deflect dykes in contrast to stiff fault zones. However, when the thickness of a fault zone is larger than 5m, dyke deflection seems to become encouraged if the fault is relatively stiff ($E \geq 1$ GPa). This result agrees with the field observations as we often observed more dyke segments deflected into thicker fault zones than thinner fault zones. Interestingly, in case studies where the thickness of the fault is less than 5m and the fault core is moderately stiff (E=1 GPa) then deflection was unlikely (Fig. 10c).

6.2.3 Local extensional (σ_{ext}) or compressional (σ_{comp}) regime, fault dip dimension (height)

It has been shown that both the local and regional stress fields contribute to dyke arrest at Santorini (Drymoni et al., 2020) and so we also investigated how a regional extensional or compressional stress field alters the interaction between dykes and faults by applying loads to vertical sides of the model. The results show that under both extensional and compressional regional stress fields, the dykes can be deflected if the fault zones are soft ($E \leq 0.1$ GPa) (Fig. 10 d and e) (S13-S18).

The different values of fault crustal dip dimension (20, 100 and 200 m) are also aiming to simulate the real height scales on Santorini volcano (S19-S21). We studied how the height of the fault can be a controlling parameter on dyke deflection. Our results have shown that if the stiffness of the fault is less than 0.1 GPa, then regardless of the fault zone height, the dykes are deflected into the fault, while the stiff fault cores cannot encourage dyke deflection irrespective of the fault height (Fig. 10f).

7. Conclusions

When approaching a fault, the likelihood that a sheet intrusion will become deflected into the fault zone depends predominantly on both the angle at which the sheet meets the fault and the mechanical properties of the fault zone. These properties and conditions presumably dominate

over small regional (remote) tension or compression, the overpressure values, and the fault dip dimension.

In Santorini, most measured fault zones are high angle (>65 degrees) and either normal or strike-slip. Therefore, there is a greater tendency for vertically propagating dykes, rather than shallow dipping inclined sheets, to become deflected into fault zones. Santorini also hosts both relatively young and active fault zones that consist of a fault core of highly brecciated and compliant or low Young's modulus material and older or inactive fault zones that host stiffer material. We find that sheet intrusions become preferentially deflected into those fault zones that contain more compliant materials. Furthermore, the thickness of both the fault zone and the sheet intrusions can also affect the potential for deflection. When the fault zone is thick compared with the sheet thickness (more than 5 times the thickness), stress rotation and deflection are usually encouraged.

More specifically, sheet intrusion deflection is encouraged when the fault core is very compliant (E<0.1 GPa). In stiffer conditions (>1 GPa), the sheet intrusions prefer to make their own paths (rupture the rock) parallel with the maximum principal compressive stress, σ_1. Vertically propagating dykes can become deflected into either homogeneous or heterogeneous fault zones, whereas inclined sheets can normally only be deflected if the fault zone is heterogeneous.

Acknowledgements

We thank the editor, D. Roman and two reviewers, A. Tibaldi and A. Geyer, for comments which helped improve this manuscript. Furthermore, we thank A. Rust & K. Cashman for helpful comments and suggestions, which significantly improved an earlier version of the manuscript. KD is grateful for a Kirsty Brown memorial fund that enabled fieldwork in the Aegean. JB acknowledges support from Fondecyt 11190143 and Fondap-Conicyt 15090013.

References

Aloisi, M., Mattia, M., Monaco, C. and Pulvirenti, F., 2011. Magma, faults, and gravitational loading at Mount Etna: The 2002–2003 eruptive period. Journal of Geophysical Research: Solid Earth, 116, B5.

Amadei, B., Stephansson, O., 1997. Rock stress and its measurement. Chapman and Hall, London.

Anderson, E.M., 1936. The dynamics of formation of cone sheets, ring dykes and cauldron subsidences. Proceedings of the royal society of Edinburgh, 56, 128-163.

Anderson, E.M., 1951. Dynamics of faulting and dyke formation, 2nd edn. Olivier and Boyd, Edinburgh.

Anderson. LJ., Osborne. R.H., Palmer. D. F., 1983. Cataclastic rocks of the San Gabriel fault-An expression of deformation at deeper crustal levels in the San Andreas fault, Tectonophysics, 98, 209-251.

Atkinson, B.K., 1987. Introduction to fracture mechanics and its geophysical applications. In: Fracture Mechanics of Rock, Ed. B. K. Atkinson. Academic Press, London. 1–26.

Atkinson, B. K., Meredith, P.G., 1987. Experimental fracture mechanics data for rocks and mineral. In: Atkinson, B.K. (ed.), Fracture Mechanics of Rock. London: Academic Press, 477-525.

Bonali, F.L., Tibaldi, A., Corazzato, C., Tormey, D.R. and Lara, L.E., 2013. Quantifying the effect of large earthquakes in promoting eruptions due to stress changes on magma pathway: the Chile case. Tectonophysics, 583, 54-67.

Broek, D., 1982. Elementary engineering fracture mechanics. Martinus Nijhoff publishers, Netherlands.

Browning J., Gudmundsson A., 2015. Caldera faults capture and deflect inclined sheets: an alternative mechanism of ring dyke formation Bull. Volcanol., 77, 1-13.

Browning, J., Drymoni K., Gudmundsson A., 2015. Forecasting magma-chamber rupture at Santorini volcano, Greece. Sci. Rep. 5, 15785.

Caine, J.S., Coates, D.R., Timofeef. N.P., and Davis, W.D., 1991. Hydrogeology of the Northern Shawangunk Mountains: New York State Geological Survey Open-File Report and maps.

Caine, J.S., Evans, J.P., Forster C.B., 1996. Fault zone architecture and permeability structure Geology. 24, 1025-1028.

Cembrano, J. and Lara, L., 2009. The link between volcanism and tectonics in the southern volcanic zone of the Chilean Andes: a review. Tectonophysics, 471, 96-113.

Chester, F.M., Logan, J.M. 1986. Implications for mechanical-properties of brittle faults from observations of the Punchbowl Fault, California, Pure Appl. Geophys., 124, 79–106.

Delaney, P., Pollard, D., Ziony, J., McKee E., 1986. Field relations between dikes and joints: emplacement processes and paleostress analysis J. Geophys. Res., 91, 4920-4938.

Delcamp, A., Troll, V.R., van Wyk de Vries, B., Carracedo, J.C., Petronis, M.S., Perez-Torrado, F.J., Deegan, F.M., 2012. Dykes and structures of the NE rift of Tenerife, Canary Islands: a record of stabilisation and destabilisation of ocean island rift zones. Bull Volcanol. 74, 5, 963–980.

Dumont, S., Socquet, A., Grandin, R., Doubre, C. and Klinger, Y., 2016. Surface displacements on faults triggered by slow magma transfers between dyke injections in the 2005–2010 rifting episode at Dabbahu–Manda–Hararo rift (Afar, Ethiopia). Geophysical Journal International, 204, 1, 399-417.

Druitt, T.H., Francaviglia, V., 1992. Caldera formation on Santorini and the physiography of the islands in the late Bronze Age. Bull. Volcanol. 54, 484-493.

Druitt, T.H., Edwards, L., Mellors, R.M., Pyle, D.M., Sparks, R.S.J., Lanphere, M., Davis, M., Barriero, B., 1999. Santorini Volcano. Geological Society Memoir No. 19, 165.

Drymoni, K., 2020. Dyke propagation paths: The movement of magma from the source to the surface. PhD thesis, University of London.

Drymoni, K., Browning, J., Gudmundsson, A., 2020. Dyke-arrest scenarios in extensional regimes: Insights from field observations and numerical models, Santorini Greece. JVGR, 396, 106854.

Faulkner, D.R., Jackson, C.A.L., Lunn, R.J., Schlische, R.W., Shipton, Z.K., Wibberley, C.A.J., Withjack, M.O., 2010. A review of recent developments concerning the structure, mechanics and fluid flow properties of fault zones, J. Struct. Geol., 32, 11, 1557–1575.

Faulkner, D.R., Mitchell, T.M., Jensen, E., Cembrano, J., 2011. Scaling of fault damage zones with displacement and the implications for fault growth processes, J. Geophys. Res.-Solid Earth 116.

Feuillet, N., 2013. The 2011–2012 unrest at Santorini rift: stress interaction between active faulting and volcanism, Geophys. Res. Lett., 40, 3532-3537.

Fourney, W.L., 1983. Fracture control blasting. In: Rossmanith, H.P. (ed.), Rock fracture Mechanics. New York: Springer-Verlag, 301-309.

Francalanci, L., Zellmer, G.F., 2019. Magma Genesis at the South Aegean Volcanic Arc. Elements 2019; 15 (3): 165–170.

Geshi, N., Browning, J. and Kusumoto, S., 2020. Magmatic overpressures, volatile exsolution and potential explosivity of fissure eruptions inferred via dike aspect ratios. Scientific Reports, 10, 1, 1-9.

Geyer, A., Gottsmann, J.H., 2008. Ground deformation at collapse calderas: influence of host rock lithology and reservoir multiplicity, IOP Conference Series: Earth and Environmental Science, 3, p. 012017.

Geyer, A., Gottsmann, J.H. 2010. The influence of mechanical stiffness on caldera deformation and implications for the 1971–1984 Rabaul uplift (Papua New Guinea). Tectonophysics, 483, 399 - 412.

Griffith, A.A., 1920. The phenomena of rupture and flow in solids. Philosophical transaction of the royal society of London, Sierres A., Containing papers of a mathematical or physical character 221, 163-198.

Griffith, A.A., 1924. The theory of rupture. In First international congress of Applied Mathematics, 55-63.

Gudmundsson, A., 1983. Form and dimensions of dykes in eastern Iceland. Tectonophysics, 95, 295-307.

947 Gudmundsson, A., 1986. Formation of dykes, feeder dykes, and the intrusion of dykes from
948 magma chambers, Bulletin of Volcanology. 47, 537-550.

949 Gudmundsson, A. 1999. Fluid overpressure and stress drop in fault zones. Geophys. Res. Lett.
950 26, 115-118.

951 Gudmundsson, A., 2011. Rock fractures in geological processes. Cambridge University Press,
952 Cambridge.

953 Gudmundsson, A., 2020. Volcanotectonics. Understanding the Structure, Deformation and
954 Dynamics of Volcanoes. Cambridge University Press, Cambridge.

955 Gudmundsson, A., Lotveit, I.F., 2012. Sills as fractured hydrocarbon reservoirs: examples and
956 models. Geological society, London, Special publications, 374, 251-271.

957 He, M.Y., Hutchinson, J.W., 1989. Crack deflection at an interface between dissimilar elastic
958 materials. Int J Solids Struct 31, 3443–3455.

959 Heap, M.J., Villeneuve, M., Albino, F., Farquharson, J.I., Brothelande, E., Amelung, F., Got,
960 J.L. and Baud, P., 2020. Towards more realistic values of elastic moduli for volcano modelling.
961 JVGR, 390,106684.

962 Hoek, H., 2000. Practical rock engineering, www.rockscience.com

963 Hutchinson, J.W., (1996). Stresses and failure modes in thin films and multilayers. Technical
964 University of Denmark-Notes for a DCAMM course.

965 Kiryukhin, A., Chernykh, E., Polyakov, A. and Solomatin, A., 2020. Magma Fracking Beneath
966 Active Volcanoes Based on Seismic Data and Hydrothermal Activity Observations.
967 Geosciences, 10, 2, 52.

968 Le Corvec, N., Menand, T., Lindsay, J., 2013. Interaction of ascending magma with pre-
969 existing crustal fractures in monogenetic basaltic volcanism: an experimental approach. J.
970 Geophys. Res. Solid Earth 118, 968–984.

971 Le Corvec, N., Muirhead, J.D. & White, J.D.L., 2018. Shallow magma diversions during
972 explosive diatreme-forming eruptions. Nature Communications, 9, 1459, 105.

973 Magee, C., Bastow, I., de Vries, B., Jackson, C., Hetherington, R., Hagos, M., & Hoggett, M.,
974 2017. Structure and dynamics of surface uplift induced by incremental sill emplacement.
975 Geology, 45, 5, 431-434.

976 Mathieu, L., van Wyk de Vries, B., Holohan, E.P., Troll, V.R., 2008. Dykes, cups saucers and
977 sills: Analogue experiments on magma intrusion into brittle rocks. Earth and Planetary Science
978 Letters, 271, 1-13.

979 Neuberg, J.W., Collinson, A.S., Mothes, P.A., Ruiz, M.C., Aguaiza, S., 2018. Understanding
980 cyclic seismicity and ground deformation patterns at volcanoes: intriguing lessons from
981 Tungurahua volcano, Ecuador. Earth Planet. Sci. Lett. 482, 193–200.

982 Ostermeijer, G.A., Mitchell, T.M., Aben, F.M., Dorsey, M.T., Browning, J., Rockwell, T.K.,
983 Fletcher, J.M. and Ostermeijer, F., 2020. Damage zone heterogeneity on seismogenic faults in
984 crystalline rock; a field study of the Borrego Fault, Baja California. Journal of Structural
985 Geology, 104016.

986 Roman, D.C., Neuberg, J., Luckett, R.R., 2006. Assessing the likelihood of volcanic eruption
987 through analysis of volcanotectonic earthquake fault-plane solutions. Earth Planet. Sci. Lett.,
988 248, 229–237.

989 Rossetti, F., Storti, F. and Salvini, F., 2000. Cenozoic noncoaxial transtension along the
990 western shoulder of the Ross Sea, Antarctica, and the emplacement of Mc Murdo dyke arrays.
991 Terra Nova, 12, 60–66.

992 Rubin, A.M., Pollard, D.D., 1987. Origins of blade-like dikes in volcanic rift zones R.W.
993 Decker, T.L. Wight, P.H. Stuffer (Eds.), Volcanism in Hawaii, US Geological Survey
994 Professional Papers, 1350, pp. 1449-1470.

995 Rubin, A.M., 1995. Propagation of magma-filled cracks. Annu. Rev. Earth Planet. Sci. 23,
996 287–336. doi: 10.1146/annurev.ea.23.050195.001443.

997 Saunders, S.J., 2004. The possible contribution of circumferential fault intrusion to caldera
998 resurgence. Bulletin of Volcanology, 67, 1, 57-71.

999 Sielfeld, G., Ruz, J., Brogi, A., Cembrano, J., Stanton-Yonge, A., Pérez-Flores, P. and Iturrieta,
1000 P., 2019. Oblique-slip tectonics in an active volcanic chain: A case study from the Southern
1001 Andes. Tectonophysics, 770, 228221.

1002 Spacapan, J.B., Galland, O., Leanza, H.A., Planke, S., 2016. Control of strike-slip fault on dyke
1003 emplacement and morphology. Journal of the Geological Society, 173, 573–576.

1004 Tibaldi, A., 1992. The role of transcurrent intra-arc tectonics in the configuration of a volcanic
1005 arc. Terra Nova, 4, 567–577.

1006 Tibaldi, A., 2015. Structure of volcano plumbing systems: A review of multi-parametric
1007 effects. J. Volcanol. Geotherm. Res. 298, 85-135.

1008 Tibaldi, A., Bonali, F.L., Corazzato, C., 2017. Structural control on volcanoes and magma
1009 paths from local-to orogen-scale: The central Andes case. Tectonophysics, 699, 16-41.

1010 van Wyk de Vries, B., Matela, R., 1998. Styles of volcano-induced deformation: numerical
1011 models of substratum flexure, spreading and extrusion. J Volcanol Geotherm Res. 81,1–18.

1012 Wang, L.P., Xu, R., 2006. Dynamic interfacial debonding initiation induced by an incident
1013 crack International Journal of Solids and Structures, 43, 6535-6550.

1014 Xu, R., Huang, Y.Y., Rosakis, A.J., 2003. Dynamic Crack Deflection and Penetration at
1015 Interfaces in Homogeneous Materials: Experimental Studies and Model Predictions Journal of
1016 the Mechanics and Physics of Solids. 51, 461-486.

1017 Zellmer, G., Blake, S., Vance, D., Hawkesworth, C., Turner, S., 1999. Plagioclase residence
1018 times at two island arc volcanoes (Kameni Islands, Santorini, and Soufrière, St. Vincent)
1019 determined by Sr diffusion systematics. Contrib. Mineral. Petrol. 136, 345–357.